Journal of Organometallic Chemistry, 383 (1990) 543–572
Elsevier Sequoia S.A., Lausanne – Printed in The Netherlands
JOM 20336

Reactions of the $[Ni_6(CO)_{12}]^{2-}$ dianion with stibine and bismuthine reagents: synthesis and stereophysical characterization of the $[Ni_{10}(SbPh)_2(CO)_{18}]^{2-}$ dianion containing a noncentered icosahedral $Ni_{10}Sb_2$ core and $Ni_2(CO)_4(\mu_2\text{-}Ph_2SbOSbPh_2)_2$ containing a centrosymmetric eight-membered $(NiSbOSb)_2$ ring *

Robert E. DesEnfants, II **, James A. Gavney, Jr., Randy K. Hayashi, A. David Rae *, Lawrence F. Dahl ***

Department of Chemistry, University of Wisconsin - Madison, Madison, Wisconsin 53706 (U.S.A.)

and Asgeir Bjarnason

Science Institute, University of Iceland, Dunhaga 3, IS-107 Reykjavik (Iceland)

(Received July 14th, 1989)

Abstract

In a further exploration of the types of high-nuclearity, mixed metal-(main-group) clusters accessible from the electron-rich $[Ni_6(CO)_{12}]^{2-}$ dianion (**1**), reactions of **1** (a direct descendent of nickel tetracarbonyl) with antimony and bismuth reagents have been carried out. The main product isolated in 50–60% yields from reactions of **1** with either chlorodiphenylstibine, Ph_2SbCl, or dichlorophenylstibine, $PhSbCl_2$, in THF solutions at room temperature is the $[Ni_{10}(SbPh)_2(CO)_{18}]^{2-}$ dianion (**2**); its identity was unambiguously established from X-ray crystallographic determinations of four different ionic compounds, viz., $[NMe_4]^+_2$ $[\mathbf{2}]^{2-} \cdot 2THF$ (**2a**), $[NMe_4]^+_2$ $[\mathbf{2}]^{2-} \cdot 2Me_2CO$ (**2b**), $[(Ph_3P)_2N]^+_2$ $[\mathbf{2}]^{2-} \cdot 2THF$ (**2c**), and $[NMe_3Ph]^+_2$ $[\mathbf{2}]^{2-}$ (**2d**). In each salt, the geometrically similar nickel stibinidene carbonyl dianion possesses a closo 1,12-disubstituted icosahedral $Ni_{10}Sb_2$ core, (i.e., a bi-Sb-capped pentagonal-antiprismatic Ni_{10} configuration) of crystallographic $C_i\text{-}\bar{1}$ site symmetry encapsulated by two antimony-attached phenyl substituents, 10 terminal carbonyl

* Presented in part at the 193rd National Meeting of the American Chemical Society, Denver, Colorado, April 5–10, 1987; American Chemical Society, Washington, DC, 1987; see R.E. DesEnfants, II, D.A. Nagaki, and L.F. Dahl, Abstracts of Papers, INOR 449.

** Present address: Department of Chemistry, New Mexico State University, Las Cruces, New Mexico 88003 (USA).

*** Present address: School of Chemistry, University of New South Wales, Kensington, New South Wales 2033 (Australia).

0022-328X/90/$03.50

ligands (one per nickel atom), and four doubly bridging and four triply bridging carbonyl ligands. This nickel-antinomy cluster is the third member of the homologous series of $[Ni_{10}(ER)_2(CO)_{18}]^{2-}$ dianions (E = P, R = Me; E = As, R = Me). A comparative geometrical analysis of their icosahedral $Ni_{10}E_2$ cores, which are electronically equivalent analogues of the regular 12-boron icosahedral polyhedron of the classic $[B_{12}H_{12}]^{2-}$ dianion, is given. The fact that **2** was the only nickel-stibinidene cluster isolated from a room-temperature reaction with Ph_2SbCl is attributed to the facile cleavage of one of the two Sb–Ph bonds of the Ph_2SbCl under the reaction conditions and to the apparent thermodynamic stability of **2**. An X-ray diffraction analysis coupled with laser desorption/Fourier transform mass spectrometry (LD/FTMS) established conclusively the formulation of a side product, obtained in ~ 5% yield from room-temperature reactions of **1** with chlorodiphenylstibine, as $Ni_2(CO)_4(\mu_2\text{-}Ph_2SbOSbPh_2)_2$ (**3**). This molecular dimer is best viewed as a disubstituted $Ni(CO)_2L_2$ derivative of nickel tetracarbonyl in which two electron-donating Sb^{III} atoms from two bridging $Ph_2SbOSbPh_2$ ligands have replaced two carbonyl ligands around each tetrahedrally-coordinated, zerovalent nickel atom. The resulting eight-membered cyclo-$(NiSbOSb)_2$ complex of crystallographic $C_i\text{-}\bar{1}$ site symmetry possesses a chair-like conformation presumably due to the bulky antimony-attached phenyl substituents. This compound (**3**) is the first example (to our knowledge) of a metal complex formed from bis(diphenylstibine)-oxide which itself exists as a molecular compound. The origin of the bridging $Ph_2SbOSbPh_2$ ligand in **3** can be readily attributed to the partial hydrolysis of the Ph_2SbCl reagent with adventitious water (i.e., "wet" solvent). The reaction of **1** with Ph_2SbCl gave a third nickel-antimony compound, $Ni(CO)_3(SbClPh_2)$: although not isolated from solution, the proposed existence of this monosubstituted derivative of $Ni(CO)_4$ is based upon its infrared carbonyl frequencies being virtually identical to those previously reported for the analogous $Ni(CO)_3(SbClEt_2)$ and $Ni(CO)_3(SbPh_3)$. Reaction of **1** with (*p*-tolyl)$BiBr_2$ in THF gave no isolatable carbonyl-containing products.

Introduction

A number of diverse types of nickel carbonyl clusters containing capping phosphinidene and arsinidene fragments have been prepared in our laboratory from reactions of the $[Ni_6(CO)_{12}]^{2-}$ dianion (**1**) [1] with dihalophosphine and dihaloarsine reagents [2–6]. The initial reaction of **1** with $PhPCl_2$ produced $Ni_8(CO)_8(\mu_4\text{-}PPh)_6$, which established the completely bonding metal cube (a Platonic solid [7]) as a basic structural unit [2]. From reactions between **1** and $^tBuPCl_2$, six different nickel t-butylphosphinidene carbonyl clusters were isolated and characterized by IR, ^1H and ^{31}P NMR, single-crystal X-ray diffraction, and cyclic voltammetry [3]. These species include: (1) two Ni_6P_4 clusters, one with a bi-P-capped, square-antiprismatic Ni_6P_2 core and the other with a tetra-P-capped trigonal-prismatic Ni_6 core, which can be interconverted to each other via decarbonylation-carbonylation reactions; (2) a Ni_9P_3 cluster possessing a cuneane-like (wedge-shaped) Ni_8 core with one $Ni(CO)_3$ and three electronically equivalent (isolobal [8]) P^tBu ligands capping the two pentagonal and two rectangular faces; (3) a Ni_8P_2 cluster containing a bi-Ni-capped square-antiprismatic Ni_6P_2 core; (4) a $Ni_{12}P_4$ cluster with an unprece-

dented "flying-saucer" D_{2d} $Ni_{12}P_4$ core; and (5) a Ni_8P_6 cluster containing a hexa-P-capped cubane Ni_8 core (i.e., an analogue of the phenylphosphinidene-capping cubane Ni_8 cluster [2]) to which an electron can be reversibly added [3,9*,10].

The first examples of a noncentered icosahedron (another Platonic solid [7]) as a fundamental building block in transition metal cluster chemistry were the Ni_9As_3 core of the $[Ni_9(AsPh)_3(CO)_{15}]^{2-}$ dianion and the $Ni_{10}As_2$ core of the $[Ni_{10}(AsMe)_2(CO)_{18}]^{2-}$ dianion isolated from the reactions of **1** with $PhAsCl_2$ and $MeAsBr_2$, respectively [4]. The homologous nickel-phosphinidene $[Ni_{12-x}(PMe)_x(CO)_{24-3x}]^{2-}$ series ($x = 2,3,4$) and the $[Ni_{12-x}(PMe)_x(CO)_{17}(\mu_2\text{-}PMe_2)]^-$ monoanion ($x = 2$) along with the hexa-P-capped cubane $Ni_8(CO)_8(\mu_4\text{-}PMe)_6$ were later isolated from reactions of **1** with $MePCl_2$ [5]. It was observed [3,5] that the particular stoichiometries and stereochemistries of the above-mentioned Ni_yE_x clusters are highly dependent on several interlocking factors: (1) electronic effects which in the case of the noncentered icosahedral $Ni_{12-x}E_x$ clusters require a valence electron count of 13 skeletal electron pairs; (2) the sizes of the different main-group E atoms relative to that of the Ni atoms; (3) steric effects arising from interligand nonbonded repulsions which dictate the number and permissible polyhedral arrangements of the carbonyl and R substituents of the ER fragments for a given core composition; and (4) the boundary conditions of a given reaction, especially the mole ratios of the reactants, giving rise to a Ni_yE_x cluster [11*–15].

The compounds reported herein are a consequence of our exploring the reactions of the $[Ni_6(CO)_{12}]^{2-}$ dianion (**1**) with halostibine and halobismuthine reagents in order to extend this area of chemistry. Species that have been spectroscopically and crystallographically characterized include the $[Ni_{10}(SbPh)_2(CO)_{18}]^{2-}$ dianion (**2**), crystallized as four different salts (**2a–2d**), and $Ni_2(CO)_4(\mu_2\text{-}Ph_2SbOSbPh_2)_2$ (**3**). The dianion (**2**) is the only nickel stibinidene carbonyl cluster isolated in this work. It was the main product from the reaction of **1** with dichlorophenylstibine and was initially crystallized and structurally characterized as the THF-solvated $[NMe_4]^+$ salt (**2a**). In an attempt to determine whether the hypothetical Ni_9Sb_3 analogue of the $[Ni_9(ER)_3(CO)_{15}]^{2-}$ dianions (E = P, R = Me [5]; E = As, R = Ph [4]) could also have been a product, $[(Ph_3P)_2N]^+Cl^-$ (where the monocation is often denoted as $[PPN]^+$) was added to the THF-soluble mixture. A structural determination identified the crystalline material obtained after removal of the solvents as the THF-solvated $[PPN]^+$ salt (**2c**) of **2**. This same dianion was also the major product of the reaction of **1** with chlorodiphenylstibine and was crystallized and analyzed as the acetone-solvated $[NMe_4]^+$ salt (**2b**). The unsolvated $[NMe_3Ph]^+$ salt (**2d**) of **2** was also the major product obtained from another reaction of **1** with chlorodiphenylstibine. Structural determinations of the four different salts (**2a–2d**) not only have allowed an assessment of the effect of crystallographic packing forces on the geometrical parameters of the $[Ni_{10}(SbPh)_2(CO)_{18}]^{2-}$ dianion (**2**) but also have enabled a comparative geometrical analysis to be made with the other two crystallographically characterized members of the homologous $[Ni_{10}(ER)_2(CO)_{18}]^{2-}$ series (E = P, R = Me [5]; E = As, R = Me [4]).

The other isolated nickel-antimony complex, $Ni_2(CO)_4(\mu_2\text{-}Ph_2SbOSbPh_2)_2$ (**3**) was obtained in ca. 5% yield from the room-temperature reaction of **1** with Ph_2SbCl

* Reference number with asterisk indicates a note in the list of references.

in THF solution. Both the composition and molecular geometry of this centrosymmetric dimer were established from an X-ray diffraction study (presented herein). The assignment of the electron-density peak connecting the two antimony atoms in each of the two centrosymmetrically related bridging $Ph_2SbOSbPh_2$ ligands as an oxygen atom was initially based upon structural-electronic considerations. Compelling crystallographic support for this assignment was obtained from anisotropic least-squares refinements, and its identity was ascertained from an analysis of laser desorption Fourier transform mass spectra. That halostibines, R_2SbX (R = alkyl, aryl), have been found [16,17] to hydrolyze to the corresponding molecular oxides, $R_2SbOSbR_2$, provides a ready explanation for the origin of $Ph_2SbOSbPh_2$, and hence of **3** as a side product. The existence of $Ph_2SbOSbPh_2$ as a molecular compound per se was initially established by Schmidt [18] in 1920 and later substantiated by Jaffe and Doak [19]. The fact that its solid-state structure was investigated by X-ray diffraction [20] and ^{121}Sb Mossbauer spectroscopy [21] has allowed a stereochemical-bonding examination (reported here) between the "free" molecule and the "ligand-bridging" entity in **3** which is the first known "adduct" complex of the "free" molecule.

Details of our attempts to isolate nickel bismuthene carbonyl clusters by reactions of **1** with a dihalobismuthine reagent, (*p*-tolyl)$BiBr_2$, are also given.

Experimental

A. Methods and materials. All reactions including sample transfers and manipulations were carried out with standard Schlenk techniques either on a preparative vacuum line under nitrogen or argon or within a Vacuum Atmospheres drybox under nitrogen.

The following solvents were freshly distilled under nitrogen from the indicated drying agent immediately prior to use: toluene (Na); hexane and cyclohexane (CaH_2); dichloromethane (P_2O_5); acetone and acetonitrile (B_2O_3); THF, benzene, diethyl ether, and diisopropyl ether (K/benzophenone); and methanol (Mg). Deuterated solvents were dried over molecular sieves, frozen and degassed three times, and finally vacuum-distilled before use. NMR samples were prepared in the drybox, transferred to a vacuum line, and then frozen and degassed three times before being hermetically sealed.

The $[Ni_6(CO)_{12}]^{2-}$ dianion (**1**) was prepared by a modification [3] of the general method of Longoni, Chini, and Cavalieri [1]. The following materials were used without further purification: $BiBr_3$ (Strem); bis(triphenylphosphoranylidene)ammonium chloride ([PPN]Cl), tetramethylammonium chloride, iodomethane, and t-BuLi (Aldrich). SiO_2 (Kieselgel 60, 230–400 mesh; Merck) was activated by heating under vacuum to 150 °C for 24 h; after being cooled to ambient temperature, distilled water (5% by weight) was added under N_2 to ensure a consistent activity. $SbPh_3$ and $SbCl_3$ (Aldrich) were sublimed prior to use.

Proton NMR spectra were recorded on either a Bruker WP-200, a Bruker AM-360, or a Bruker AM-500 spectrometer and were referenced indirectly to tetramethylsilane by use of residual solvent protons. ^{13}C NMR spectra were recorded on a Bruker AM-500 spectrometer at 125 MHz, and were referenced indirectly to tetramethylsilane.

Infrared spectra were obtained on a Beckman Model IR-4240 spectrophotometer. Solution spectra were obtained by use of nitrogen-purged CaF_2 cells, while solid-state samples were prepared in the drybox as KBr disks; their spectra were recorded immediately after their removal from the drybox.

Electrochemical measurements were performed with a Bioanalytical Systems Electrochemical Analyzer (BAS-100) equipped with a Princeton Applied Research (PAR) electrochemical cell enclosed in a N_2-filled Vacuum Atmospheres drybox. The cell consisted of a platinum disk working electrode and a coiled platinum wire counter electrode. The reference electrode was a porous Vycor-tipped aqueous saturated calomel electrode separated from the test solution by a Vycor-tipped salt bridge with a 0.1 *M* tetra-n-butylammonium hexafluorophosphate/CH_3CN filling solution. The top of the salt bridge was situated ca. 5 mm from the working electrode. Solution volumes were ca. 5 ml with a sample concentration of ca. 10^{-3} *M*. An *iR* compensation for solution resistance was made before measurement of the current vs. voltage curves.

Mass spectra were obtained by use of a Nicolet FTMS-2000 Fourier transform mass spectrometer equipped with a 3.0-tesla superconducting magnet, a Nicolet laser desorption interface, and a Tachisto 215G CO_2 pulsed infrared laser operated as an aperture-controlled stable resonator. Each sample (0.01 to 0.1 mg) was dissolved in methanol or dichloromethane, and a few drops of the solution were allowed to evaporate on the stainless steel tip of the direct insertion probe of the mass spectrometer. The laser was focused onto the probe tip to give an estimated spot size of approximately 100 microns with an estimated output energy of approximately 0.01–0.05 J/pulse. The probe was rotated several degrees after each laser shot such that the laser always struck a new spot on the sample layer. A five-second delay-time between each laser shot and ion detection was used so that spectral quality was not reduced by the effects of the pressure burst accompanying the laser desorption. During each delay-time the ions produced in the laser desorption process were stored in the cell of the spectrometer. Room-temperature electron impact (EI) spectra were obtained on the same instrument by use of the same sample-handling technique. The background pressure in the mass spectrometer was well below 10^{-8} torr for each of the LD/FT and EI/FT mass spectral measurements. Mass spectra were recorded in both the positive- and negative-ion modes. Peak assignments were based on exact mass determinations, isotope distribution patterns, and fragmentation plausibility.

B. Preparation of $PhSbCl_2$. The synthetic procedure of Wieber et al. [22] was essentially utilized. A solution of $SbPh_3$ (3.0 g; 8.5 mmol) in 50 ml of degassed, dry Et_2O was added via a stainless-steel cannula to a 250 ml round bottom flask (RBF) containing $SbCl_3$ (3.89 g 17.0 mmol) dissolved in 25 ml of Et_2O. The colorless solution was refluxed with stirring for 30 h and then stirred at room temperature for 40 h. Removal of the solvent in vacuo gave a viscous yellow oil, which crystallized under vacuum after approximately 24 h. The crude crystalline $PhSbCl_2$ was loaded into a water-cooled sublimator in the drybox and then placed on a high-vacuum line. The solid melted at about 50 °C (10^{-4} torr) and distilled onto the sublimator probe forming oily, colorless crystals in 90% yield. The colorless solid was stored in the Vacuum Atmospheres drybox at −30 °C. At room temperature, even in the drybox, the solid turned to a pinkish color after a few days. M.p. 52–55 °C (uncorrected). ^1H NMR (acetone-d_6): δ 7.47 (m, 3 H), 8.04 (m, 2 H). Positive-ion

LD/FT mass spectrum; prominent ion peaks correspond to the molecular parent ion, $[M]^+$, at m/z 268/270, $[SbCl_2]^+$ at m/z 191/193, $[SbCl]^+$ at m/z 156/158, and $[Sb]^+$ at m/z 121/123.

C. Preparation of Ph_2SbCl. This compound was prepared analogously to $PhSbCl_2$ except that the ratio of $SbCl_3$ to $SbPh_3$ was 1/2 [22]. In a typical reaction, $SbCl_3$ (5.7 g; 25 mmol) in 50 ml of Et_2O was added via cannula to $SbPh_3$ (17.65 g; 50 mmol) in 50 ml of Et_2O. This solution was refluxed with stirring for 15 h and then stirred at room temperature for 96 h. The solvent was removed in vacuo to give a yellow oil which crystallized with difficulty in vacuo. The crude solid Ph_2SbCl was loaded into a sublimator inside the drybox. The sublimator was removed from the drybox, attached to a high vacuum line, brought to vacuum (10^{-4} torr), and heated with an oil bath. The solid melted at about 50 °C and distilled onto the water-cooled condenser as oily colorless crystals (21 g, 90% yield) leaving behind a thick yellow oil. Ph_2SbCl must also be stored at −30 °C in the drybox to prevent a gradual yellowing of the product. M.p. 46–48 °C. ^1H NMR (acetone-d_6): δ 7.41 (m, 3 H), 7.76 (m, 2 H).

*D. Reaction of $[NMe_4]^+_2[Ni_6(CO)_{12}]^{2-}$ with dichlorophenylstibine, $PhSbCl_2$: isolation of $[NMe_4]^+_2[Ni_{10}(SbPh)_2(CO)_{18}]^{2-} \cdot 2THF$ (**2a**) and $[PPN]^+_2[Ni_{10}(SbPh)_2(CO)_{18}]^{2-} \cdot 2THF$ (**2c**).* A solution of $PhSbCl_2$ (0.322 g, 1.2 mmol) in 10 ml of THF was added slowly over five minutes with a cannula to $[NMe_4]^+_2[Ni_6(CO)_{12}]^{2-}$ (0.5 g; 0.6 mmol) slurried in 40 ml of THF contained in a 100 ml RBF under N_2. The solution darkened immediately from cherry-red to deep red-brown. An infrared spectrum showed the disappearance of the characteristic carbonyl stretching bands due to the $[Ni_6(CO)_{12}]^{2-}$ dianion (**1**) and the appearance of new bands in both the terminal and bridging carbonyl stretching regions.

After 2 h, the red-brown solution was filtered from an insoluble green powder (presumably $NiCl_2$) which was discarded. Removal of the solvent in vacuo from the red-brown solution gave a brown powder. This powder was extracted successively with hexane, toluene, and THF. The hexane extracts were colorless. Only a small fraction dissolved in toluene to give a dark brown solution. This brown toluene extract was concentrated and loaded onto a toluene/SiO_2 chromatographic column under N_2. Solutions of the products from the column deposited solids over time, indicating poor stability in solution. Attempts to crystallize these products via vapor diffusion, solvent layering, and cooling failed. IR (THF): 2080(vw), 2035(s), 2015(sh), 1960(m), 1820(m) cm^{-1}.

The majority of the powder dissolved in THF to give a deep red-brown solution. When the solvent was removed in vacuo from the THF extract, 250 mg of brown powder was isolated. An estimated yield of 50% is based on the reaction:

$$2\left[Ni_6(CO)_{12}\right]^{2-} + 2PhSbCl_2 \rightarrow$$

$$\left[Ni_{10}(SbPh)_2(CO)_{18}\right]^{2-} + Ni(CO)_4 + NiCl_2 + 2Cl^- + 2CO$$

A concentrated THF solution of the brown powder was crystallized (over several days) via layering with cyclohexane. Suitable single crystals were obtained and identified as $[NMe_4]^+_2[Ni_{10}(SbPh)_2(CO)_{18}]^{2-} \cdot 2THF$ (**2a**) from an X-ray diffraction investigation (vide infra). IR (THF): 2020(s), 1840(m), 1780(w,sh) cm^{-1} (Fig. 1). IR (KBr pellet): 1985(s), 1825(m), 1750(m) cm^{-1}.

$[PPN]^+Cl^-$ was added to the THF extract containing the brown powder in an attempt to fractionally crystallize as the $[PPN]^+$ salt any other anions, in particular

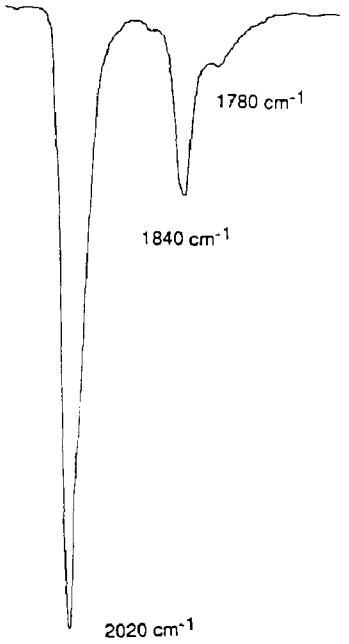

Fig. 1. Infrared spectrum in the carbonyl region for the $[Ni_{10}(SbPh)_2(CO)_{18}]^{2-}$ dianion (**2**) in THF solution. The three observed bands at 2020, 1840, and 1780 cm^{-1} are assigned as terminal, doubly bridging, and triply bridging carbonyl stretching modes, respectively, in accordance with the solid-state arrangement of carbonyl ligands about the icosahedral $Ni_{10}Sb_2$ core.

the hypothetical $[Ni_9(SbPh)_3(CO)_{15}]^{2-}$ and/or $[Ni_8(SbPh)_4(CO)_{12}]^{2-}$ dianions, which might form along with **2**. However, only the THF solvated $[PPN]^+$ salt (**2c**) of the $Ni_{10}Sb_2$ dianion was isolated.

*E. Attempted protonation and carbon-insertion reactions with the $[Ni_{10}(SbPh)_2(CO)_{18}]^{2-}$ dianion (**2a**).* The following two reactions with **2a** were carried out: (1) A 1.2 *M* solution of HCl(aq) (0.25 ml; 0.3 mmol) was added via a syringe to $[NMe_4]^+_2[Ni_{10}(SbPh)_2(CO)_{18}]^{2-}$ (250 mg; 0.14 mmol) dissolved in 20 ml of THF. The reactants were stirred at room temperature for two days. Infrared spectra taken periodically showed no significant changes in the carbonyl stretching region, and 240 mg of **2a** were recovered upon solvent removal. (2) Solid CBr_4 (24 mg, 0.07 mmol) was added to $[NMe_4]^+_2[Ni_{10}(SbPh)_2(CO)_{18}]^{2-}$ (240 mg; 0.13 mmol) dissolved in 25 ml of THF in an attempt to form an interstitial carbide cluster. This mixture was stirred at 45–50 °C for 6 h and then at room temperature for an additional four days. A series of infrared spectra of the reaction mixture showed the carbonyl absorptions of the starting material and of the decomposition product, $Ni(CO)_4$.

*F. Reactions of $[NMe_3Ph]^+$ and $[NMe_4]^+$ salts of the $[Ni_6(CO)_{12}]^{2-}$ dianion with chlorodiphenylstibine, Ph_2SbCl: isolation of $[NMe_3Ph]^+_2[Ni_{10}(SbPh)_2(CO)_{18}]^{2-}$ (**2d**), $[NMe_4]^+_2[Ni_{10}(SbPh)_2(CO)_{18}]^{2-}\cdot 2Me_2CO$ (**2b**), and $Ni_2(CO)_4(\mu_2\text{-}Ph_2SbOSbPh_2)_2$ (**3**).* A solution of Ph_2SbCl (0.65 g; 2.08 mmol) in 20 ml of THF was added slowly via a cannula to $[NMe_3Ph]^+_2[Ni_6(CO)_{12}]^{2-}$ (1.0 g; 1.04 mmol) slurried in 80 ml of THF. During the addition, the reaction mixture turned from cherry-red to brown. The solution was stirred at room temperature for 2 h. An infrared spectrum showed the disappearance of the characteristic carbonyl stretch-

ing bands of the $[Ni_6(CO)_{12}]^{2-}$ dianion (**1**) and the appearance of new bands in both the terminal and bridging regions. Solvent removal in vacuo left an oily brown residue, from which successive extractions were performed with hexane, toluene, and THF.

The major product isolated from this reaction, $[NMe_3Ph]^+_2[Ni_{10}(SbPh)_2(CO)_{18}]^{2-}$ (**2d**) was obtained in 50–60% yields from the THF extract. Its spectral properties closely resembled those given for **2a**. Its formulation was unambiguously determined from an X-ray crystallographic study (vide infra). Similarly, the dianion **2** was also obtained as the main product from the reaction of the corresponding $[NMe_4]^+$ salt of **1** with Ph_2SbCl. Removal of the solvent from the THF extract followed by crystallization from an acetone solution gave $[NMe_4]^+_2[Ni_{10}(SbPh)_2(CO)_{18}]^{2-} \cdot 2Me_2CO$ (**2b**) in ca. 48% yield. Its formulation was obtained from an X-ray crystallographic study (vide infra).

The initial hexane extraction of the brown powder isolated from the reaction of Ph_2SbCl with either the $[NMe_3Ph]^+$ or $[NMe_4]^+$ salt of **1** gave in each case $Ni(CO)_3(SbClPh_2)$, whose existence was inferred from infrared data, and $Ni_2(CO)_4(\mu_2\text{-}Ph_2SbOSbPh_2)_2$ (**3**), a hydrolyzed product, which was isolated and crystallographically characterized. Pale yellow crystals of **3** were obtained (yield, ~ 5%) by slow evaporation of the hexane solvent from the yellow solution. THF and CH_2Cl_2 solutions of **3** were very air-sensitive and eventually decomposed to an unidentified black powder.

Proton NMR spectra (CD_2Cl_2) of **3** gave a single resonance at: δ 7.35 (m, 40 H). $^{13}C\{^1H\}$ NMR spectra (CD_2Cl_2) of **3** exhibited resonances indicative of two distinct isomers. Major isomer: δ 129.24 (C-*meta*, 16C), 129.6 (C-*para*, 8C), 135.6 (C-*ortho*, 16C), 135.7 (C–Sb, 8C). Minor isomer: δ 128.9 (C-*para*, 8C), 129.16 (C-*meta*, 16C), 136.5 (C-*ortho*, 16C), 139.0 (C–Sb, 8C). M.p. (sealed tube) 118–123°C (decomp.).

An infrared spectrum (Fig. 2) of the products extracted with hexane gave several carbonyl absorption bands at 2075(m), 2040(m), 2020(sh), 2005(s), and 1970(w) cm^{-1}. The frequency at 2040 cm^{-1} is readily assigned to the carbonyl stretching mode of $Ni(CO)_4$ [25]. On the other hand, an infrared spectrum (Fig. 3) of crystals of **3** dissolved in THF gave two very strong bands at 2015 and 1960 cm^{-1} and a very weak band at 2078 cm^{-1}. This latter two-band spectrum (Fig. 3) is characteristic of a disubstituted $Ni(CO)_2L_2$ complex, for which group theoretical considerations [25,26] based on localized C_{2v} symmetry lead to the prediction of two vibrational C–O stretching modes ($A_1 + B_1$) which are IR active. The higher frequency of 2015 cm^{-1} is readily assigned to the symmetrical stretching nickel dicarbonyl mode (A_1) and the lower frequency of 1960 cm^{-1} to the corresponding antisymmetrical mode (B_1). Furthermore, these two observed frequencies for **3** are in remarkably close agreement with the corresponding frequencies of 2016 and 1963 cm^{-1} reported [26] for $Ni(CO)_2(SbPh_3)_2$. The markedly different spectrum (Fig. 2) based on the hexane extract points to the primary product (in addition to **3** which accounts for the weak bands at 2020 and 1970 cm^{-1}) in solution being $Ni(CO)_3(SbClPh_2)$. This tentative identification is based upon the two remaining bands at 2075(m) and 2005(s) cm^{-1} closely resembling those of 2082(m) and 2009(s) cm^{-1} reported [26] for $Ni(CO)_3(SbClEt_2)$. The corresponding observed frequencies (and assignments under C_{3v} symmetry) for $Ni(CO)_3(SbPh_3)$ are 2074 (A_1) and 2004.5 (E) cm^{-1} [26].

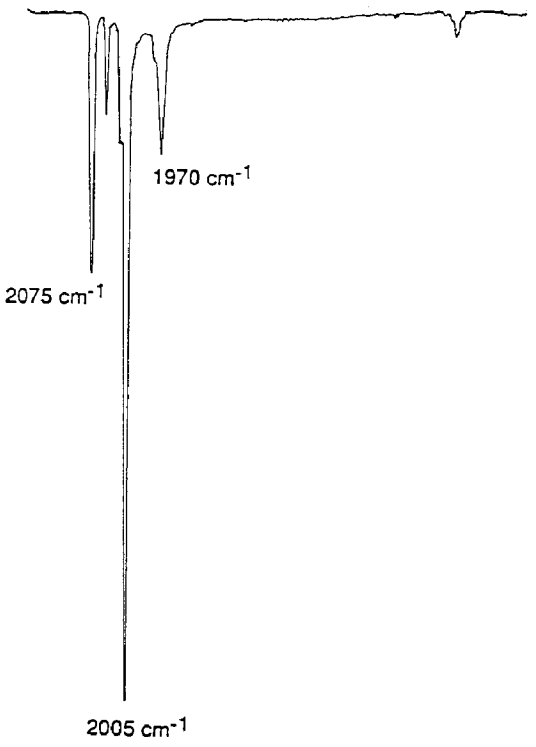

Fig. 2. Infrared spectrum in the carbonyl region for the hexane extract from the room-temperature reaction of $[Ni_6(CO)_{12}]^{2-}$ dianion (**1**) with Ph_2SbCl. Relatively strong bands at 2075 and 2005 cm^{-1} are assigned to $Ni(CO)_3(SbClPh_2)$, the weaker bands at 2020 and 1970 cm^{-1} to $Ni_2(CO)_4(\mu_2\text{-}Ph_2SbOSbPh_2)$ (**3**), and the band at 2040 cm^{-1} to $Ni(CO)_4$. These assignments are based upon comparative infrared spectra either of these species per se and/or of closely related species.

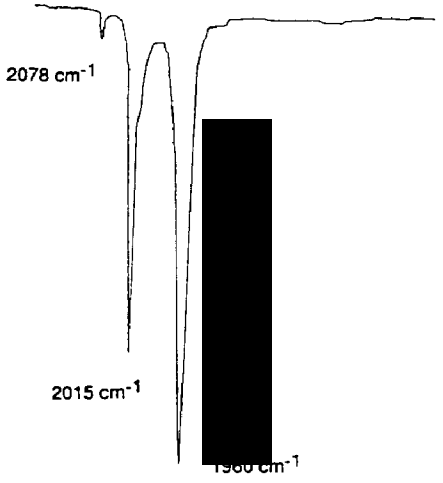

Fig. 3. Infrared spectrum in the carbonyl region for $Ni_2(CO)_4(\mu_2\text{-}Ph_2SbOSbPh_2)_2$ (**3**) in THF solution. The two strong carbonyl absorption bands at 2015 and 1960 cm^{-1} are virtually identical with corresponding frequencies of 2016 and 1963 cm^{-1} reported [26] for $Ni(CO)_2(SbPh_3)_2$.

Cyclic voltammetric measurements showed that in THF solution **3** undergoes only irreversible oxidation. The formulation of this compound was based upon an X-ray crystallographic study coupled with a detailed mass spectral analysis (vide infra).

G. Mass spectral analysis of $Ni_2(CO)_4(\mu_2\text{-}Ph_2SbOSbPh_2)_2$ *(3).* Mass spectra obtained from a Nicolet FTMS-2000 spectrometer in both electron impact (EI) and laser desorption (LD) modes identified the two centrosymmetrically- related diantimony-connecting groups in the cyclic molecule as oxygen atoms.

Positive-ion EI mass spectra with high signal-to-noise peaks were obtained, but they provided no useful information concerning the nature of the diantimony-bridging groups. The ions assigned from the major peaks observed in the 70-eV positive-ion EI spectrum are $[SbPh]^+$ at *m/z* 198/200, $[Sb]^+$ at *m/z* 121/123, and $[Ph]^+$ at *m/z* 77. Positive-ion EI mass spectra at 20, 10, and 7 eV gave an additional peak, assigned as $[SbPh_3]^+$, at *m/z* 352/354. Negative-ion EI spectra and spectra obtained after reaction delay-times between ion formation and detection to facilitate self-chemical ionization (self-CI) yielded no additional data.

Laser desorption/Fourier transform mass spectrometry (LD/FTMS) of both pure **3** and **3** doped with KBr was carried out. Positive- and negative-ion LD/FT mass spectra were recorded, in which such parameters as sample concentration, laser power, and delay-time before ion detection (after each laser shot) were varied in order to optimize spectral quality. Although neither the molecular ion, $[M]^+$, nor pseudomolecular ions of **3** were observed, both negative- and positive-ion LD/FT spectra provided several major peaks readily assignable as monooxygen-containing ions. Of prime significance were the peaks displayed by the negative-ion mass spectra at *m/z* 291/293 and *m/z* 377/379/381 which were readily attributed to the $[SbPh_2O]^-$ and $[SbPh_2ONi(CO)]^-$ ions, respectively. These particular ion fragments are cleavage products from **3** without rearrangements. These results are completely consistent with the X-ray crystallographic analysis (vide infra) in unambiguously establishing an oxygen linkage between each of the two pairs of antimony atoms in **3**.

H. Preparation of $(p\text{-tolyl})_3Bi$. The procedure described below is a modification of those given in the literature [23,24a]. A 2.2 *M* solution of t-BuLi (62 ml, 136 mmol) in n-pentane was transferred via a cannula into 30 ml of THF at −78°C. *p*-bromotoluene (11.7 g; 68 mmol) in 50 ml of THF at −78°C was added over 30 minutes to the t-BuLi solution. A milky white solid precipitated from the yellow solution during addition. The temperature was raised to 0°C, and the solution became homogeneous again. The temperature was then lowered to −78°C, and $BiBr_3$ (10 g; 22 mmol) in 50 ml of THF was added slowly via a cannula. The reaction mixture turned brown, and a brown precipitate settled to the bottom of the flask. A finely divided brown solid was left upon solvent removal. This solid was extracted with dichloromethane in a soxhlet extractor. Removal of the solvent from the colorless filtrate gave white needles which were recrystallized from an acetone/Et_2O mixture. The resulting quantity (3.95 g) of $(p\text{-tolyl})_3Bi$ corresponded to a 37% yield. ^1H NMR ($CDCl_3$): δ 2.30 (s, CH_3-Ph, 9H) 7.17 (d, $^3J(H_o\text{-}H_m)$ 8.3 Hz, *o*-C_6H_4, 6H) 7.60 (d, $^3J(H_o\text{-}H_m)$ 8.3 Hz, *m*-C_6H_4, 6H). M.p. 116–117°C (uncorrected).

I. Preparation of $(p\text{-tolyl})BiBr_2$. This procedure is closely related to those given in the literature [23,24b]. Yellow $BiBr_3$ (2 g; 4.6 mmol) was dissolved in 30 ml of

Et_2O to form a colorless solution. Bi(*p*-tolyl)$_3$ (1.08 g; 2.23 mmol) in 30 ml of Et_2O was added via cannula over five minutes to the $BiBr_3$ solution. A yellow precipitate formed during the addition.The solvent was removed, and the resulting yellow powder (2.3 g; yield, 75%) was dried in vacuo. M.p. 222–224°C (decomp., sealed tube).

J. Reaction of (p-tolyl)BiBr$_2$ with [NMe$_3$Ph]$^+_2$[Ni$_6$(CO)$_{12}$]$^{2-}$. $[NMe_3Ph]^+_2[Ni_6(CO)_{12}]^{2-}$ (0.64 g, 0.67 mmol) was slurried in 100 ml of THF at −78°C, after which (*p*-tolyl)$BiBr_2$ (0.7 g; 1.52 mmol) was added with a spatula in several portions to give a dark red solution. An infrared spectrum of the reaction mixture at room temperature showed a large peak at 2040 cm^{-1} indicative of the presence of $Ni(CO)_4$. The solvent was removed at 0°C. Extracts of the gray residue with hexane and toluene were colorless, and an infrared spectrum was featureless. Extraction with THF gave a small amount of a yellow-brown solution which precipitated over time as a gray powder. Extraction with acetonitrile gave no further products. Hence, no stable carbonyl-containing products were isolated from this reaction.

K. Structural determinations and refinements.

(a) General. Each crystal was mounted under argon inside a Lindemann glass capillary which was hermetically sealed. A refurbished Siemens-Nicolet $P\bar{1}$ diffractometer with graphite-monochromatized Mo-K_α radiation was used to collect intensity data for the four different salts (**2a**, **2b**, **2c**, and **2d**) of the $[Ni_{10}(SbPh)_2(CO)_{18}]^{2-}$ dianion (**2**) and for the structural determination of $Ni_2(CO)_4(\mu_2\text{-}Ph_2SbOSbPh_2)_2$ (**3**). The unit-cell dimensions for each structure were derived from a least-squares analysis of setting angles for 15–25 well-centered reflections obtained from either a rotation photograph or a thin shell of higher angle data collected at maximum scan speed. Axial photographs were taken to verify lattice lengths and cell symmetry. Intensities of three standard reflections periodically measured after every 47 reflections for each crystal showed no significant variations during data collection for any of the crystal structures. Empirical absorption corrections were applied to each data set [27*–29]. Neutral atomic scattering factors with corrections for anomalous dispersion were taken from the International Tables for X-Ray Crystallography [30].

(b) Analysis of [NMe$_4$]$^+_2$[Ni$_{10}$(SbPh)$_2$(CO)$_{18}$]$^{2-}$ · 2THF (2a). Crystals were obtained from the layering of cyclohexane onto a concentrated solution of **2a** in THF. Intensities were obtained for two independent monoclinic octants from a parallelepiped-shaped crystal (of approximate dimensions $0.15 \times 0.3 \times 0.7$ mm) at −100°C. Crystal data together with data-collection and least-squares refinement parameters are given in Table 1. Observed systematic absences of $\{h0l\}$ for $h + l$ odd and $\{0k0\}$ for k odd uniquely define the probable space group to be $P2_1/n$. This centrosymmetric space group, which was substantiated by the successful structural determination and refinement, results in the two $[Ni_{10}(SbPh)_2(CO)_{18}]^{2-}$ dianions each possessing crystallographic C_i-$\bar{1}$ site symmetry and the four tetramethylammonium cations and four tetrahydrofuran molecules possessing general C_1-1 site symmetry.

Initial positions for the one independent antimony atom capping a pentagon of five independent nickel atoms were determined by direct methods [31]. The resulting centrosymmetric $Ni_{10}Sb_2$ core conforms to an icosahedral framework. The remaining nonhydrogen atoms were found from successive difference maps coupled with

Table 1

Crystal data, data-collection and refinement parameters for the $[Ni_{10}(SbPh)_2(CO)_{18}]^{2-}$ dianion (**2**) as $[NMe_4]^+_2[\mathbf{2}]^{2-}\cdot 2THF$ (**2a**); $[NMe_4]^+_2[\mathbf{2}]^{2-}\cdot 2Me_2CO$ (**2b**); $[PPN]^+_2[\mathbf{2}]^{2-}\cdot 2THF$ (**2c**); $[NMe_3Ph]^+_2[\mathbf{2}]^{2-}$ (**2d**)

Compound	**2a**	**2b**	**2c**	**2d**
Formula weight (g/mol)	1781.51	1753.46	2710.39	1777.44
Crystal system	monoclinic	triclinic	triclinic	triclinic
a (Å)	21.351(8)	10.102(3)	13.667(5)	10.934(6)
b (Å)	12.895(5)	11.097(5)	14.483(6)	13.077(8)
c (Å)	11.105(6)	12.645(5)	15.156(6)	10.319(5)
α (deg)	90.00(–)	90.18(3)	115.20(3)	89.64(5)
β (deg)	96.45(4)	90.70(3)	94.03(4)	92.84(4)
γ (deg)	90.00(–)	93.59(3)	93.17(4)	108.61(4)
V (Å^3)	3029 (2)	1415 (1)	2687 (2)	1396 (1)
Temperature (°C)	−100	−100	−100	−100
Space group	$P2_1/n$	$P\bar{1}$	$P\bar{1}$	$P\bar{1}$
Z	2	1	1	1
d_{calcd} (g/cm^3)	1.95	2.06	1.67	2.11
μ_{calcd} (cm^{-1})	39.7	42.8	23.1	43.0
Scan mode	ω	θ–2θ	θ–2θ	θ–2θ
2θ limits (deg)	3–55	4–50	3–35	3–45
Scan speed (deg/min)	4–24	4–29.3	4–29.3	2–24
No. check refl/freq	3/47	3/47	3/47	3/47
No. data collected	3869	5752	3866	4153
No. indep data $\|F\| > 3\sigma(F)$	2346	4262	2987	2445
No. parameters refined	282	340	579	347
Data/parameter ratio	8.3/1	12.4/1	5.2/1	7.0/1
$R_1(F)$ [a]	4.60	4.01	2.98	7.30
$R_2(F)$ [a]	6.55	4.81	4.23	8.29
Goodness-of-fit (GOF) [a]	–	1.21	0.86	1.25

[a] $R_1(F) = [\Sigma\|\|F_o\| - \|F_c\|\|/\Sigma|F_o|]\cdot 100$; $R_2(F) = [\Sigma w_i\|\|F_o\| - \|F_c\|\|^2/\Sigma w_i|F_o|^2]^{1/2}\cdot 100$; and GOF $= [\Sigma w_i\|\|F_o\| - \|F_c\|\|^2/(m-n)]^{1/2}\cdot 100$; where $w_i = [\sigma^2(F) + 0.0009F^2]^{-1}$, m is number of independent data, and n is number of variable parameters.

isotropic least-squares refinement. The tetramethylammonium cation, the antimony-attached phenyl substituent, and the THF molecule of crystallization were refined as rigid groups with hydrogen atoms included at idealized positions [32]. Full-matrix least-squares refinement with RAELS [29] converged at $R_1(F)$ 4.60% and $R_2(F)$ 6.55% with a data-to-parameter ratio of 8.3/1. The largest parameter change-to-esd ratio in the final least-squares cycle was 0.5. A final difference map showed no unusual features.

*(c) $[NMe_4]^+_2[Ni_{10}(SbPh)_2(CO)_{18}]^{2-}\cdot 2Me_2CO$ (**2b**).* Crystals were obtained by the layering of diisopropyl ether over a concentrated solution of **2b** in acetone. Intensities were measured at −100 °C for four independent triclinic octants from a parallelepiped-shaped crystal (of approximate dimensions $0.3 \times 0.4 \times 0.7$ mm). Crystal data along with data-collection and refinement parameters are given in Table 1. The successful structural determination and refinement under centrosymmetric $P\bar{1}$ symmetry necessitates that the crystallographically independent unit be composed of one-half of the dianion (**2**) along with one tetramethylammonium cation and one solvated acetone molecule.

The positions of the independent antimony atom and the five independent Ni atoms were found by direct methods. The remaining nonhydrogen atoms were found from successive difference Fourier syntheses coupled with isotropic least-squares refinement. The phenyl substituent on the antimony atom was refined as a rigid group in which all hydrogen atoms were included in idealized positions with fixed isotropic thermal parameters. Anisotropic least-squares refinement converged at $R_1(F)$ 4.0%, $R_2(F)$ 4.8%, with a goodness-of-fit value of 1.207. A final difference map showed no abnormal features with the largest positive residual peak of 1.4 e/Å^3 located at 0.96 Å from Sb(1). The largest parameter change-to-esd ratio in the final cycle was 0.023. Positional and equivalent isotropic thermal parameters for the nonhydrogen atoms are given in Table 2 and anisotropic thermal parameters are listed in Table 3. Selected interatomic distances are presented in Table 4. All computations were performed on a Data General Eclipse S/140 system with the SHELXTL (1984) program package.

(d) Analysis of $[PPN]^+_2[Ni_{10}(SbPh)_2(CO)_{18}]^{2-} \cdot 2THF$ *(2c).* Crystals were obtained by layering a concentrated THF solution of **2c** with cyclohexane. Intensities were measured at $-100\,^\circ$C for four independent triclinic octants from a rod-shaped crystal (of approximate dimensions $0.2 \times 0.3 \times 0.5$ mm). Crystal data together with data collection and least-squares refinement parameters are listed in Table 1. The structure was determined and refined under centrosymmetric $P\bar{1}$ symmetry which requires that one-half the dianion (**1**), one $[(PPN)]^+$ monocation, and one solvated THF molecule make up the crystallographically independent part of the unit cell.

Preliminary positions for the independent antimony and five independent Ni atoms were located by direct methods. The remaining nonhydrogen atoms were found from successive difference maps coupled with isotropic least-squares refinement. The one antimony-attached and six phosphorus-attached phenyl rings were each refined as a rigid group. All hydrogen atoms were included in idealized positions with fixed isotropic thermal parameters. Least-squares refinement converged at $R_1(F)$ 2.98%, $R_2(F)$ 4.23%, and a goodness-of-fit value of 0.86. A final difference map exhibited no unusual features. The largest positive residual peak was only 0.3 e$^-$/Å^3. The largest parameter change-to-esd ratio in the final cycle was 0.153. All computations were performed on a Data General Eclipse S/140 system with the SHELXTL(1984) program package.

(e) Analysis of $[NMe_3Ph]^+_2[Ni_{10}(SbPh)_2(CO)_{18}]^{2-}$ *(2d).* Crystals were obtained by a layering of cyclohexane on a concentrated solution of **2d** in THF. Intensities were measured at $-100\,^\circ$C for four independent triclinic octants from an irregularly shaped crystal (of approximate dimensions $0.1 \times 0.2 \times 0.3$ mm). Crystal data and data-collection parameters are given in Table 1. The determined structure is based on centrosymmetric $P\bar{1}$ symmetry, under which one-half of a dianion (**2**) and one $[NPh_3Me]^+$ monocation constitute the crystallographically independent unit.

Initial positions for the independent antimony and five nickel atoms were determined by direct methods. All other nonhydrogen atoms were located from successive difference syntheses. The antimony-attached and the nitrogen-attached phenyl rings were each refined as a rigid group. All hydrogen atoms were included in idealized positions and refined to a common isotropic thermal parameter. Least-squares refinement converged at $R_1(F)$ 7.30%, $R_2(F)$ 8.29%, and a goodness-of-fit value of 1.25. A final difference map exhibited no unusual features. The

(continued on p. 558)

Table 2. Atomic coordinates ($\times 10^4$) and equivalent isotropic thermal parameters ($Å^2 \times 10^4$) for $[NMe_4]^+_2[Ni_{10}(SbPh)_2(CO)_{18}]^{2-} \cdot 2Me_2CO$ (**2b**)

	x	y	z	U_{eq}
Sb(1)	5383(1)	1198(1)	1114(1)	144(1)
Ni(1)	2911(1)	552(1)	1005(1)	159(2)
Ni(2)	4906(1)	−907(1)	1863(1)	159(2)
Ni(3)	7232(1)	−257(1)	966(1)	163(2)
Ni(4)	6838(1)	1610(1)	−485(1)	159(2)
Ni(5)	4278(1)	2110(1)	−499(1)	162(2)
C(1)	2467(7)	1469(6)	2083(5)	224(20)
O(1)	2167(6)	2012(6)	2803(4)	412(20)
C(2)	4453(7)	−683(6)	3200(5)	227(21)
O(2)	4049(6)	−548(6)	4028(4)	432(21)
C(3)	8463(7)	500(7)	1817(6)	246(21)
O(3)	9235(5)	1021(6)	2319(5)	411(19)
C(4)	7899(7)	2771(6)	134(5)	211(20)
O(4)	8578(5)	3464(5)	536(5)	362(18)
C(5)	3688(7)	3537(7)	−176(6)	267(22)
O(5)	3291(6)	4458(5)	−41(5)	432(20)
C(13)	1650(7)	1070(7)	−35(5)	233(21)
O(13)	717(5)	1605(5)	−46(4)	337(17)
C(14)	2054(7)	−930(6)	1480(5)	219(20)
O(14)	1272(5)	−1219(5)	2112(4)	325(17)
C(235)	3297(7)	1666(6)	−1821(5)	209(20)
O(235)	2749(5)	2205(5)	−2465(4)	281(16)
C(245)	5820(7)	2527(6)	−1503(6)	224(20)
O(245)	6060(5)	3428(4)	−1976(4)	267(15)
Ph(1)	5556(5)	3691(4)	2272(3)	277(22)
Ph(2)	5821	4499	3106	352(25)
Ph(3)	6352	4095	4055	319(24)
Ph(4)	6618	2884	4170	293(23)
Ph(5)	6353	2076	3335	245(21)
Ph(6)	5822	2480	2386	173(18)
N(1)	9571(6)	4750(6)	−2658(5)	258(18)
Me(1)	10431(10)	3936(8)	−2083(8)	490(32)
Me(2)	10422(9)	5744(9)	−3166(7)	515(33)
Me(3)	8772(8)	4065(9)	−3487(7)	417(28)
Me(4)	8669(8)	5300(9)	−1889(7)	451(30)
C(10)	1992(8)	2423(8)	5183(6)	322(24)
C(11)	3427(8)	2431(8)	5080(7)	405(28)
C(12)	1248(12)	1254(10)	5343(9)	692(43)
O(10)	1420(6)	3342(6)	5160(5)	477(22)
H(1)	5191	3969	1619	800
H(2)	5638	5333	3028	800
H(3)	6534	4651	4630	800
H(4)	6983	2606	4823	800
H(5)	6535	1242	3414	800
He(1A)	11013	3580	−2573	800
He(1B)	9892	3311	−1744	800
He(1C)	10949	4389	−1558	800
He(2A)	9868	6275	−3540	800
He(2B)	11018	5400	−3651	800
He(2C)	10923	6190	−2628	800
He(3A)	8218	4603	−3854	800
He(3B)	8228	3434	−3161	800
He(3C)	9356	3718	−3981	800

Table 2 (continued)

	x	y	z	U_{eq}
He(4A)	8107	5830	−2257	800
He(4B)	9189	5751	−1365	800
He(4C)	8132	4672	−1551	800
H(11A)	3699	1619	5119	800
H(11B)	3847	2904	5641	800
H(11C)	3680	2775	4411	800
H(12A)	1850	619	5343	800
H(12B)	608	1119	4781	800
H(12C)	800	1263	6007	800

Table 3. Anisotropic thermal parameters ($Å^2 \times 10^4$) for $[NMe_4]^+_2[Ni_{10}(SbPh)_2(CO)_{18}]^{2-} \cdot 2Me_2CO$ (**2b**)

	U_{11}	U_{22}	U_{33}	U_{23}	U_{13}	U_{12}
Sb(1)	149(2)	141(2)	141(2)	−2(2)	1(2)	9(2)
Ni(1)	151(4)	160(4)	167(4)	−7(3)	14(3)	16(3)
Ni(2)	177(4)	153(4)	150(4)	2(3)	12(3)	18(3)
Ni(3)	146(4)	176(4)	167(4)	−2(3)	1(3)	14(3)
Ni(4)	150(4)	152(4)	174(4)	−8(3)	9(3)	0(3)
Ni(5)	174(4)	150(4)	165(4)	5(3)	2(3)	24(3)
C(1)	199(33)	234(36)	241(37)	28(30)	2(28)	16(28)
O(1)	452(34)	489(36)	304(30)	−183(28)	46(26)	106(29)
C(2)	304(37)	173(34)	206(37)	22(28)	−9(29)	21(29)
O(2)	613(39)	475(37)	223(30)	−12(26)	92(27)	134(31)
C(3)	222(35)	256(37)	271(37)	12(31)	68(30)	84(30)
O(3)	244(28)	537(38)	444(34)	−201(30)	−77(25)	−10(26)
C(4)	187(32)	232(36)	221(34)	−6(29)	19(27)	65(28)
O(4)	329(29)	285(29)	461(33)	−139(26)	−100(26)	−52(24)
C(5)	242(36)	324(43)	234(36)	54(31)	−2(29)	19(32)
O(5)	523(37)	295(32)	508(37)	−68(27)	50(29)	261(28)
C(13)	205(34)	302(39)	187(33)	−12(29)	5(27)	−12(30)
O(13)	286(28)	454(33)	293(28)	−40(25)	17(22)	211(26)
C(14)	202(33)	212(35)	243(35)	34(29)	54(28)	−9(27)
O(14)	339(29)	252(28)	382(30)	17(23)	182(25)	−38(23)
C(235)	198(32)	219(35)	208(34)	57(28)	25(27)	−13(27)
O(235)	284(27)	296(28)	271(27)	28(22)	−56(22)	82(22)
C(245)	257(34)	173(35)	245(35)	−60(29)	−17(28)	44(28)
O(245)	235(25)	244(27)	321(28)	102(23)	13(21)	12(21)
Ph(1)	374(41)	212(36)	243(37)	−55(30)	−87(31)	25(31)
Ph(2)	442(46)	219(39)	393(46)	−89(34)	−93(37)	25(34)
Ph(3)	332(40)	295(41)	328(41)	−106(33)	10(33)	19(33)
Ph(4)	292(38)	347(42)	223(36)	16(32)	−33(30)	−97(33)
Ph(5)	247(35)	306(40)	175(33)	10(30)	13(27)	−32(30)
Ph(6)	157(30)	204(34)	153(31)	−36(26)	28(24)	−36(25)
N(1)	236(30)	278(33)	261(31)	19(26)	23(25)	24(25)
Me(1)	540(56)	316(47)	620(62)	−64(43)	−201(48)	114(42)
Me(2)	467(53)	664(67)	384(50)	153(46)	45(41)	−218(49)
Me(3)	343(43)	572(58)	323(44)	−72(41)	11(35)	−62(40)
Me(4)	322(43)	528(56)	502(54)	−201(45)	42(39)	28(40)
C(10)	355(42)	391(46)	212(37)	−52(33)	21(31)	−30(36)
C(11)	353(44)	482(53)	389(47)	−69(40)	−8(36)	93(39)
C(12)	817(81)	591(69)	622(69)	−64(56)	162(60)	−337(61)
O(10)	443(35)	525(40)	481(37)	−29(31)	9(29)	169(31)

The anisotropic displacement exponent takes the form:
$-2\pi^2(h^2a \times^2 U_{11} + \ldots + 2hka \times b \times U_{12})$

Table 4

Selected interatomic distances for the closo-1,12-disubstituted icosahedral $Ni_{10}Sb_2$ core in the centrosymmetric $[Ni_{10}(SbPh)_2(CO)_{18}]^{2-}$ dianion (**2**) as $[NMe_4]^+_2[\mathbf{2}]^{2-}\cdot 2THF$ (**2a**); $[NMe_4]^+_2[\mathbf{2}]^{2-}\cdot 2Me_2CO$ (**2b**); $[PPN]^+_2[\mathbf{2}]^{2-}\cdot 2THF$ (**2c**); $[NMe_3Ph]^+_2[\mathbf{2}]^{2-}$ (**2d**)

	2a	**2b**	**2c**	**2d**
A. Distances (Å) between centrosymmetrically related core atoms				
Ni(1)–Ni(1a)	5.203(7)	5.163(2)	5.225(3)	5.223(5)
Ni(2)–Ni(2a)	5.124(5)	5.131(2)	5.153(3)	5.148(5)
Ni(3)–Ni(3a)	5.165(5)	5.167(2)	5.182(3)	5.167(5)
Ni(4)–Ni(4a)	5.145(5)	5.151(2)	5.180(3)	5.192(5)
Ni(5)–Ni(5a)	5.154(5)	5.147(2)	5.185(3)	5.155(5)
	5.16 (av)	5.15 (av)	5.19 (av)	5.18 (av)
Sb(1)–Sb(1a)	3.904(4)	3.905(2)	3.889(2)	3.946(4)
B. Ni–Sb distances (Å)				
Ni(1)–Sb(1)	2.561(2)	2.556(1)	2.572(1)	2.581(3)
Ni(2)–Sb(1)	2.541(2)	2.543(1)	2.554(1)	2.559(3)
Ni(3)–Sb(1)	2.557(2)	2.553(1)	2.573(1)	2.575(3)
Ni(4)–Sb(1)	2.531(2)	2.541(1)	2.560(1)	2.560(3)
Ni(5)–Sb(1)	2.552(2)	2.556(1)	2.561(1)	2.564(3)
	2.55 (av)	2.55 (av)	2.56 (av)	2.57 (av)
C. Intrapentagonal Ni–Ni distances (Å)				
Ni(1)–Ni(2)	2.870(2)	2.868(1)	2.882(2)	2.861(4)
Ni(2)–Ni(3)	2.680(2)	2.681(1)	2.707(1)	2.705(3)
Ni(3)–Ni(4)	2.799(2)	2.816(1)	2.833(1)	2.823(4)
Ni(4)–Ni(5)	2.689(2)	2.679(1)	2.722(2)	2.700(3)
Ni(5)–Ni(1)	2.884(2)	2.881(1)	2.88791)	2.908(4)
	2.78 (av)	2.78 (av)	2.81 (av)	2.80 (av)
D. Interpentagonal Ni–Ni distances (Å)				
Ni(1)–Ni(3a)	2.518(2)	2.514(1)	2.520(1)	2.528(3)
Ni(1)–Ni(4a)	2.518(3)	2.514(1)	2.524(1)	2.531(3)
Ni(2)–Ni(4a)	2.555(4)	2.548(1)	2.541(1)	2.558(3)
Ni(2)–Ni(5a)	2.370(2)	2.366(2)	2.397(1)	2.381(3)
Ni(3)–Ni(5a)	2.543(3)	2.546(1)	2.533(1)	2.533(3)
	2.50 (av)	2.50 (av)	2.50 (av)	2.51 (av)

largest positive residual peak was 1.09 e/Å^3. The largest parameter change-to-esd ratio in the final cycle was 0.167. All computations were performed on a Data General Eclipse S/140 system with the SHELXTL (1984) program package.

(f) Analysis of $Ni_2(CO)_4(\mu_2\text{-}Ph_2SbOSbPh_2)_2$ (3). Crystals of **3** were obtained by the cooling of a concentrated hexane solution to $-20\,^\circ$C for several days. Intensities were measured at ambient temperature (ca. 18 °C) for two independent monoclinic octants from a plate-like crystal (of approximate dimensions $0.1 \times 0.3 \times 0.4$ mm). Crystal data along with data-collection and refinement parameters are listed in Table 5. Systematic absences uniquely defined the monoclinic space group as $P2_1/n$.

Compound **3** was found to possess crystallographic C_i-$\bar{1}$ site symmetry such that one nickel, two antimony, and one oxygen atoms comprise the independent half of

Table 5

Crystal data, data-collection and refinement parameters for $Ni_2(CO)_4(\mu_2\text{-}Ph_2SbOSbPh_2)_2$ (3)

Formula weight (g/mole)	1365.31
Crystal system	monoclinic
a, b, c (Å)	12.1870(2), 15.5393(3), 13.2431(3)
β (deg); V (Å^3)	90.37(1); 2508(1)
Temperature (°C)	−100
Space group	$P2_1/n$
Z	2
d_{calcd} (g/cm^3)	1.82
μ_{calcd} (cm^{-1})	29.4
Scan mode	Wyckoff ω
2θ limits (deg)	3–55
Scan speed (deg/min)	4–29.3
No. check refl/freq	3/47
No. data collected	6579
No. indep data $\|F\| > 3\sigma(F)$	3872
No. parameters refined	241
Data/parameter ratio	16.1/1
$R_1(F)$, $R_2(F)$, GOF	5.72, 6.83, 1.027

an eight-membered $(NiSbOSb)_2$ ring. Initial positions for the nickel atom and two antimony atoms were determined by application of the direct-methods program RANT [33]. The remaining nonhydrogen atomic positions including those for the two independent carbonyl and four independent phenyl ring substituents were determined from successive difference maps coupled with isotropic least-squares refinement in which each phenyl ring was constrained to a regular hexagon with a C–C bond length of 1.395 Å; hydrogen atoms were included in idealized positions at a C–H distance of 0.96 Å. Anisotropic least-squares refinement converged at $R_1(F)$ 5.72%, $R_2(F)$ 6.83%, and a goodness-of-fit value of 1.027. The largest parameter change-to-esd ratio for the final cycle was 0.015. A final difference map revealed no anomalous features; the magnitude of the largest positive residual peak was only 0.79 e$^-$/Å^3. Atomic positional parameters and equivalent isotropic thermal parameters for the nonhydrogen atoms are given in Table 6, and atomic anisotropic thermal parameters are listed in Table 7. Interatomic distances and bond angles are presented in Table 8.

Our initial assignment of the peak bridging the two antimony atoms as an oxygen atom was based upon structural-electronic considerations. Convincing evidence for this formulation of **3** was provided from least-squares refinements. When this ring atom was designated as an oxygen, the equivalent isotropic thermal parameter (U) acquired from the anisotropic refinement conformed to a physically meaningful value (Table 6) in that it was larger than those of the two independent antimony atoms but smaller than those for the carbonyl carbon and oxygen atoms. A separate refinement in which the bridging ligand was assumed to be an isoelectronic CH_2 group yielded a physically unacceptable small equivalent isotropic thermal parameter (i.e., significantly smaller than any of the other atomic U values in the structure) because of the insufficient electron-density for the bridging atom. These results are also consistent with the relative sizes, shapes, and orientations of the atomic thermal

Table 6

Atomic coordinates ($\times 10^4$) and equivalent isotropic thermal parameters ($Å^2 \times 10^3$) for $Ni_2(CO)_4(\mu_2\text{-}Ph_2SbOSbPh_2)_2$ (3)

	x	y	z	U_{eq}
Sb(1)	−1891(1)	−557(1)	−348(1)	42(1)
Sb(2)	666(1)	−1301(1)	1395(1)	41(1)
Ni(1)	−1307(1)	−984(1)	1354(1)	44(1)
C(1)	−1605(9)	−142(8)	2212(8)	61(4)
O(1)	−1859(8)	347(6)	2812(7)	98(4)
C(2)	−1904(8)	−1996(8)	1625(8)	61(4)
O(2)	−2281(8)	−2636(6)	1835(7)	103(4)
C(3)	−1582(5)	−974(4)	−2621(5)	58(4)
C(4)	−1123	−1397	−3449	75(5)
C(5)	−249	−1967	−3304	82(5)
C(6)	167	−2113	−2333	96(6)
C(7)	−292	−1690	−1506	77(5)
C(8)	−1167	−1120	−1650	43(3)
C(9)	−4151(6)	−21(4)	−1219(6)	69(4)
C(10)	−5239	−149	−1525	80(5)
C(11)	−5731	−954	−1402	76(5)
C(12)	−5134	−1632	−974	71(4)
C(13)	−4046	−1505	−669	63(4)
C(14)	−3555	−699	−791	46(3)
C(15)	2507(5)	−1572(5)	2978(5)	68(4)
C(16)	2999	−1511	3931	90(6)
C(17)	2397	−1205	4751	95(6)
C(18)	1303	−959	4617	88(6)
C(19)	810	−1020	3663	73(5)
C(20)	1412	−1326	2844	51(3)
C(21)	1850(6)	−2509(4)	−96(5)	63(4)
C(22)	2048	−3289	−589	85(5)
C(23)	1581	−4049	−227	95(6)
C(24)	915	−4030	628	94(6)
C(25)	717	−3250	1121	71(4)
C(26)	1184	−2490	759	48(3)
O(3)	1804(5)	−656(4)	699(5)	56(2)
H(3)	−2184	−582	−2721	90
H(4)	−1409	−1297	−4117	90
H(5)	67	−2259	−3874	90
H(6)	769	−2506	−2234	90
H(7)	−6	−1790	−838	90
H(9)	−3813	533	−1304	90
H(10)	−5650	318	−1819	90
H(11)	−6480	−1042	−1612	90
H(12)	−5473	−2187	−890	90
H(13)	−3636	−1971	−374	90
H(15)	2921	−1783	2414	90
H(16)	3753	−1680	4023	90
H(17)	2736	−1163	5407	90
H(18)	888	−748	5181	90
H(19)	57	−851	3571	90
H(21)	2171	−1986	−346	90
H(22)	2507	−3302	−1178	90
H(23)	1718	−4585	−566	90
H(24)	594	−4553	878	90
H(25)	258	−3237	1709	90

Table 7

Anisotropic thermal parameters ($Å^2 \times 10^3$) for $Ni_2(CO)_4(\mu_2\text{-}Ph_2SbOSbPh_2)_2$ (3)

	U_{11}	U_{22}	U_{33}	U_{23}	U_{13}	U_{12}
Sb(1)	41(1)	44(1)	42(1)	1(1)	−0(1)	−0(1)
Sb(2)	43(1)	39(1)	42(1)	−0(1)	0(1)	−0(1)
Ni(1)	43(1)	48(1)	42(1)	−1(1)	4(1)	−1(1)
C(1)	58(6)	70(7)	53(6)	−15(5)	8(5)	12(5)
O(1)	113(7)	99(7)	84(6)	−35(6)	7(5)	27(6)
C(2)	53(6)	63(7)	67(7)	4(6)	6(5)	−8(5)
O(2)	109(7)	79(6)	120(8)	12(6)	15(6)	−49(6)
C(3)	56(6)	63(7)	53(6)	4(5)	−13(5)	7(5)
C(4)	85(9)	96(100)	44(6)	−8(6)	−6(5)	−4(7)
C(5)	79(8)	113(11)	54(7)	−16(7)	17(6)	4(8)
C(6)	85(9)	128(13)	74(8)	−17(8)	7(7)	30(9)
C(7)	72(7)	104(10)	55(6)	−10(6)	7(5)	34(7)
C(8)	38(5)	40(5)	51(5)	3(4)	−2(4)	2(4)
C(9)	64(7)	65(8)	77(8)	2(6)	1(6)	5(6)
C(10)	51(7)	101(10)	88(9)	19(8)	−10(6)	14(7)
C(11)	33(5)	104(10)	91(9)	−20(8)	−14(5)	−4(6)
C(12)	52(6)	58(7)	102(9)	−7(7)	8(6)	−4(5)
C(13)	42(5)	57(7)	89(8)	−7(6)	−10(5)	−0(5)
C(14)	39(5)	51(6)	47(5)	−6(4)	6(4)	−2(4)
C(15)	80(8)	54(7)	70(7)	−3(5)	−18(6)	1(6)
C(16)	96(10)	77(9)	95(10)	7(8)	−51(8)	1(8)
C(17)	146(14)	71(9)	69(9)	7(7)	−40(9)	−20(9)
C(18)	153(14)	70(8)	41(6)	0(6)	−3(7)	−7(9)
C(19)	96(9)	68(8)	55(7)	0(6)	7(6)	−4(7)
C(20)	63(6)	52(6)	38(5)	5(4)	−10(4)	−15(5)
C(21)	69(7)	62(7)	57(6)	−3(5)	0(5)	20(6)
C(22)	117(11)	76(9)	64(7)	−6(7)	−0(7)	32(8)
C(23)	115(12)	71(9)	98(10)	−27(8)	−22(9)	32(9)
C(24)	115(12)	46(7)	121(12)	−7(8)	−6(10)	−12(8)
C(25)	73(8)	47(7)	93(9)	−3(6)	7(6)	−1(6)
C(26)	47(5)	43(5)	54(5)	4(4)	−5(4)	8(4)
O(3)	50(4)	51(4)	66(4)	5(3)	3(3)	1(3)

ellipsoids obtained from the anisotropic refinement based on the assignment of an oxygen scattering factor for the diantimony-connecting ring atom.

Results and discussion

Isolation and characterization of the $[Ni_{10}(SbPh)_2(CO)_{18}]^{2-}$ dianion (2). The main product isolated in 50–60% yields from reactions of the $[Ni_6(CO)_{12}]^{2-}$ dianion (**1**) with either chlorodiphenylstibine, Ph_2ClSb, or dichlorophenylstibine, $PhCl_2Sb$, in THF solutions at room temperature is the $[Ni_{10}(SbPh)_2(CO)_{18}]^{2-}$ dianion (**2**). Its identity was established from X-ray crystallographic determinations of four different ionic compounds-viz. $[NMe_4]^+_2[\mathbf{2}]^{2-} \cdot 2THF$ (**2a**), $[NMe_4]^+_2[\mathbf{2}]^{2-} \cdot 2Me_2CO$ (**2b**), $[(Ph_3P)_2N]^+_2[\mathbf{2}]^{2-} \cdot 2THF$ (**2c**), and $[NMe_3Ph]^+_2[\mathbf{2}]^{2-}$ (**2d**).

Table 4 reveals that the corresponding distances within the $Ni_{10}Sb_2$ core in **2** for the four different salts (**2a–2d**) are remarkably alike. The carbonyl ligand arrangement is also unchanged, and the corresponding carbonyl distances and bond angles

Table 8

Intramolecular distances and bond angles for $Ni_2(CO)_4(\mu_2\text{-}Ph_2SbOSbPh_2)_2$ (**3**)

Bond lengths (Å)			
Sb(1)–Ni(1)	2.447(1)	Sb(1)–C(8)	2.126(6)
Sb(1)–C(14)	2.114(7)	Sb(1)–O(3A)	1.941(7)
Sb(2)–Ni(1)	2.450(1)	Sb(2)–C(20)	2.114(7)
Sb(2)–C(26)	2.124(7)	Sb(2)–O(3)	1.944(7)
Ni(1)–C(1)	1.770(11)	Ni(1)–C(2)	1.766(12)
C(1)–O(1)	1.140(15)	C(2)–O(2)	1.129(15)
O(3)–Sb(1A)	1.941(7)		
Bond angles (°)			
Ni(1)–Sb(1)–C(8)	120.9(2)	Ni(1)–Sb(1)–C(14)	119.9(2)
C(8)–Sb(1)–C(14)	97.7(3)	Ni(1)–Sb(1)–O(3A)	117.8(2)
C(8)–Sb(1)–O(3A)	100.4(3)	C(14)–Sb(1)–O(3A)	95.0(2)
Ni(1)–Sb(2)–C(20)	116.0(2)	Ni(1)–Sb(2)–C(26)	117.3(2)
C(20)–Sb(2)–C(26)	102.5(3)	Ni(1)–Sb(2)–O(3)	126.0(2)
C(20)–Sb(2)–O(3)	97.8(3)	C(26)–Sb(2)–O(3)	92.6(3)
Sb(1)–Ni(1)–Sb(2)	110.7(1)	Sb(1)–Ni(1)–C(1)	109.3(4)
Sb(2)–Ni(1)–C(1)	109.8(3)	Sb(1)–Ni(1)–C(2)	108.0(4)
Sb(2)–Ni(1)–C(2)	102.8(3)	C(1)–Ni(1)–C(2)	116.1(5)
Sb(1)–C(8)–C(3)	121.9(2)	Sb(1)–C(8)–C(7)	118.0(2)
Sb(1)–C(14)–C(9)	121.9(2)	Sb(1)–C(14)–C(13)	118.1(2)
Sb(2)–C(20)–C(15)	121.6(2)	Sb(2)–C(20)–C(19)	118.2(2)
Sb(2)–C(26)–C(21)	120.9(2)	Sb(2)–C(26)–C(25)	118.4(2)
Ni(1)–C(1)–O(1)	173.5(10)	Ni(1)–C(2)–O(2)	177.5(11)
Sb(2)–O(3)–Sb(1A)	130.7(3)		

are essentially invariant within experimental errors. These results support the premise that interionic packing interactions (which are dissimilar for the four salts) do not have a significant influence on either the configuration or dimensions of the dianion. Since the structural determination of the $[NMe_4]^+_2[Ni_{10}(SbPh)_2(CO)_{18}]^{2-} \cdot 2Me_2CO$ (**2b**) yielded the most precise dimensions, as evidenced directly by the smallest esd's (Table 4) and indirectly by the relatively high data-to-parameter ratio and low discrepancy indicies (Table 1), the crystallographic data are presented herein only for this salt.

An infrared spectrum (Fig. 1) of **2** in THF solution displays a characteristic three-band pattern resembling that obtained for the $[Ni_{10}(PMe)_2(CO)_{18}]^{2-}$ homologue [5]. Based upon the structural determination of **2**, the strong band at 2020 cm^{-1} is ascribed to the ten terminal carbonyl ligands, the medium band at 1840 cm^{-1} to the four doubly bridging carbonyl ligands, and the weak, partially resolved band at 1780 cm^{-1} to the four triply bridging carbonyl ligands.

Attempts to isolate other possible anions, in particular the hypothetical $[Ni_9(SbPh)_3(CO)_{15}]^{2-}$ and $[Ni_8(SbPh)_4(CO)_{12}]^{2-}$ dianions (i.e., homologues of the known Ni_9E_3 (E = P, As) and Ni_8P_4 clusters) which might be formed along with **2**, were unsuccessful. Since either of these hypothetical dianions would possess direct Sb–Sb bonding, their presumed nonexistence (at least under our reaction conditions) may be rationalized on the basis of both bond-energy and covalent size considerations which readily lead to the prediction of much greater instability of icosahedral Ni_9E_3 and Ni_8E_4 cores for E = Sb than for E = P.

(continued on p. 565)

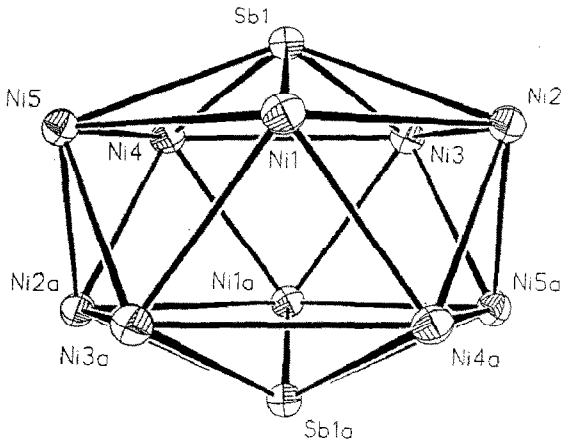

Fig. 4. The icosahedral $Ni_{10}Sb_2$ core in the $[Ni_{10}(\mu_5\text{-}SbPh)_2(CO)_{18}]^{2-}$ dianion of the acetone-solvated $[NMe_4]^+$ salt (**2b**). The anisotropic thermal ellipsoids are drawn at the 50% probability level.

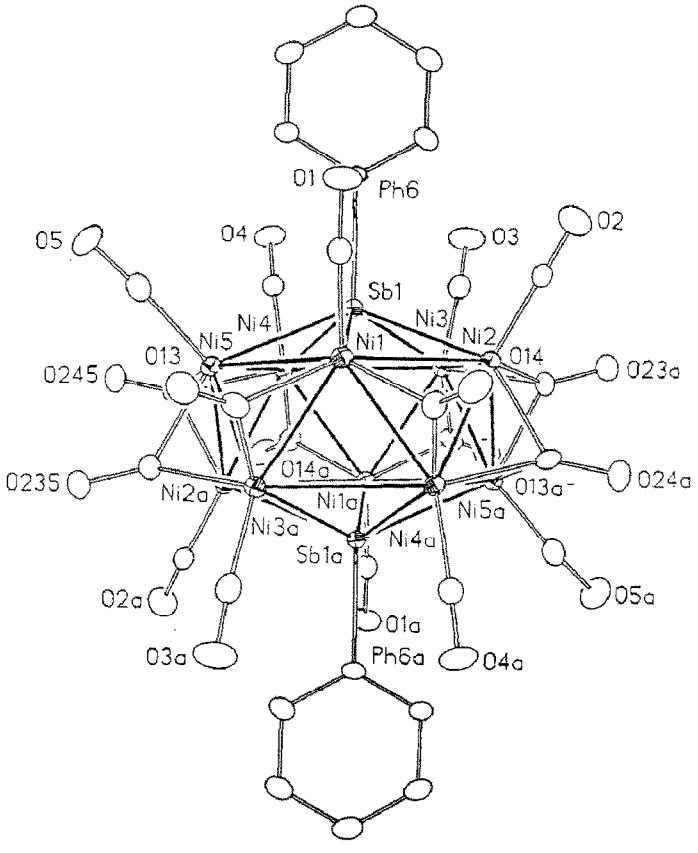

Fig. 5. Configuration of the $[Ni_{10}(SbPh)_2(CO)_{18}]^{2-}$ dianion of the acetone-solvated $[NMe_4]^+$ salt (**2b**). The entire dianion of crystallographic C_i-$\bar{1}$ site symmetry closely conforms to C_{2h}-$2/m$ symmetry with the pseudo mirror plane passing through Ni(1), Ni(1a), Sb(1), Sb(1a) and symmetry relating the Ni(2), Ni(5) atoms and the Ni(3), Ni(4) atoms. The anisotropic thermal ellipsoids are drawn at the 35% probability level.

Table 9

Comparative geometrical analysis of the centrosymmetric $[Ni_{10}(ER)_2(CO)_{18}]^{2-}$ homologues (E = P, R = Me [a]; E = As, R = Me [b]; E = Sb, R = Ph [c]) under assumed D_{5d}-$\overline{1}0$ 2 m symmetry [d]

	$Ni_{10}P_2$	$Ni_{10}As_2$	$Ni_{10}Sb_2$
A. Distances (Å) between centrosymmetrically related core atoms			
Ni(1)–Ni(1a)	4.900(2)	5.043(3)	5.163(2)
Ni(2)–Ni(2a)	4.857(2)	4.974(3)	5.131(2)
Ni(3)–Ni(3a)	4.929(2)	5.034(3)	5.167(2)
Ni(4)–Ni(4a)	4.970(2)	5.037(3)	5.151(2)
Ni(5)–Ni(5a)	4.862(2)	4.957(3)	5.147(2)
	4.90 (av)	5.01 (av)	5.15 (av)
E(1)–E(1a)	3.168(2)	3.689(2)	3.905(2)
B. Ni–E distances (Å)			
Ni(1)–E(1)	2.364(2)	2.450(2)	2.556(1)
Ni(2)–E(1)	2.353(2)	2.412(2)	2.543(1)
Ni(3)–E(1)	2.344(2)	2.431(2)	2.553(1)
Ni(4)–E(1)	2.343(2)	2.440(2)	2.541(1)
Ni(5)–E(1)	2.338(2)	2.405(2)	2.556(1)
	2.35 (av)	2.43 (av)	2.55 (av)
C. Intrapentagonal Ni–Ni distances (Å)			
Ni(1)–Ni(2)	2.655(1)	2.731(2)	2.868(1)
Ni(2)–Ni(3)	2.563(2)	2.635(2)	2.681(1)
Ni(3)–Ni(4)	2.615(2)	2.712(2)	2.816(1)
Ni(4)–Ni(5)	2.563(2)	2.621(2)	2.679(1)
Ni(5)–Ni(1)	2.650(2)	2.731(2)	2.881(1)
	2.61 (av)	2.69 (av)	2.78 (av)
D. Interpentagonal Ni–Ni distances (Å)			
Ni(1)–Ni(3a)	2.495(2)	2.502(2)	2.514(1)
Ni(1)–Ni(4a)	2.521(2)	2.500(2)	2.514(1)
Ni(2)–Ni(4a)	2.538(2)	2.510(2)	2.548(1)
Ni(2)–Ni(5a)	2.389(1)	2.417(1)	2.366(1)
Ni(3)–Ni(5a)	2.531(2)	2.522(2)	2.546(1)
	2.50 (av)	2.49 (av)	2.50 (av)
E. Ni–CO (bridging) distances (Å)			
Ni(1)–C(13)	1.917(7)	1.93(1)	1.934(7)
Ni(1)–C(14)	1.944(8)	1.90(1)	1.911(7)
Ni(3)–C(13)	1.900(7)	1.86(1)	1.905(7)
Ni(4)–C(14)	1.898(8)	1.90(1)	1.882(7)
Ni(2)–C(235)	2.034(7)	2.26(1)	2.050(7)
Ni(2)–C(245)	1.971(9)	1.90(1)	1.950(7)
Ni(3)–C(235)	1.974(7)	1.95(1)	1.954(7)
Ni(4)–C(245)	1.953(7)	1.96(1)	1.964(7)
Ni(5)–C(235)	2.007(7)	1.91(1)	1.978(7)
Ni(5)–C(245)	2.084(8)	2.19(1)	2.053(7)

Table 9 (continued)

	$Ni_{10}P_2$	$Ni_{10}As_2$	$Ni_{10}Sb_2$
F. Ni–CO (terminal) distances (Å)			
Ni(1)–C(1)	1.791(8)	1.81(1)	1.778(7)
Ni(2)–C(2)	1.766(7)	1.76(1)	1.777(7)
Ni(3)–C(3)	1.784(9)	1.78(1)	1.800(7)
Ni(4)–C(4)	1.790(8)	1.77(1)	1.795(7)
Ni(5)–C(5)	1.768(7)	1.76(1)	1.775(8)
	1.78 (av)	1.78 (av)	1.78 (av)
G. C–O (bridging) distances (Å)			
C(13)–O(13)	1.17(1)	1.17(1)	1.145(9)
C(14)–O(14)	1.15(1)	1.15(1)	1.162(9)
C(235)–O(235)	1.17(1)	1.17(1)	1.166(8)
C(245)–O(245)	1.18(1)	1.20(1)	1.180(8)
H. C–O (terminal) distances (Å)			
C(1)–O(1)	1.14(1)	1.11(1)	1.145(9)
C(2)–O(2)	1.13(1)	1.12(1)	1.142(9)
C(3)–O(3)	1.12(1)	1.13(1)	1.129(9)
C(4)–O(4)	1.12(1)	1.15(1)	1.115(8)
C(5)–O(5)	1.14(1)	1.12(1)	1.134(10)
	1.13 (av)	1.13 (av)	1.13 (av)
I. E–R distance (Å)			
P–C(Me)	1.881(8)	–	–
As–C(Me)	–	1.99(1)	–
Sb–C(Ph)	–	–	2.167(4)

[a] $[PPN]^+$ salt; ref. 5. [b] $[NMe_4]^+$ salt; ref. 4, 5b. [c] Acetone-solvated $[NMe_4]^+$ salt; this work. [d] The pseudo principal fivefold axis passes through E(1) and E(1a).

Structural features of the $[Ni_{10}(SbPh)_2(CO)_{18}]^{2-}$ dianion (2). The icosahedral $Ni_{10}Sb_2$ core in **2** can be viewed as a pentagonal antiprism of ten nickel atoms which are capped on the upper and lower pentagonal faces with antimony atoms (Fig. 4 and 5).

The only crystallographically imposed symmetry on the dianion in each salt is a center of symmetry, but the entire dianion closely approximates C_{2h}-2/*m* site symmetry. As expected for a heteroatomic $Ni_{10}Sb_2$ core, the dianion (**2**) is significantly distorted from a regular icosahedron of I_h symmetry by a compression along the pseudo fivefold axis passing through Sb(1) and Sb(1a). This distortion is easily seen from a comparison of the nonbonded distances between opposite pairs of core atoms (Tables 4 and 9). Whereas the five centrosymmetrically related pairs of Ni atoms in **2b** are all within 0.02 Å of the mean value of 5.15 Å, the Sb–Sb distance of 3.905(2) Å is 1.25 Å shorter.

Each Ni atom of the dianion has a terminal carbonyl ligand with an average Ni–C bond length of 1.78 Å. There are eight nearly symmetrical bridging carbonyl ligands (Table 9), of which four are doubly bridging (mean Ni–C distance, 1.91 Å; range, 1.882(7)–1.934(7) Å) and four are triply bridging (mean Ni–C distance, 1.99 Å; range, 1.950(7)–2.053(7) Å). Figure 5 gives a view of the pseudo C_{2h} ligand arrangement surrounding the $Ni_{10}Sb_2$ core; the eight bridging carbonyl ligands

connect the two antimony capped nickel pentagons either by spanning interpentagonal edges or by capping triangular faces.

Geometrical comparison of the $[Ni_{10}(ER)_2(CO)_{18}]^{2-}$ dianions (E = P, As, Sb) and resulting implications. A tabulation of the corresponding interatomic distances under assumed D_{5d}-$\overline{1}0$ 2 *m* symmetry is given in Table 9 for the members of the $[Ni_{10}(ER)_2(CO)_{18}]^{2-}$ series (E = P, As, R = Me; E = Sb, R = Ph). A comparative analysis reveals the following interrelationships: (1) The five independent Ni–E(1) distances expectedly increase in accordance with the increased size of the E atom. Subtraction of the tetrahedral covalent radii for P (1.10 Å), As (1.22 Å), and Sb (1.42 Å) from the mean Ni–E(1) distance yields values of 1.25, 1.21, and 1.13 Å for the covalent nickel radius. (2) The icosahedral $Ni_{10}E_2$ core is similarly deformed for all three members by a large compression along the pseudo fivefold E(1)–E(1a) axis. The observed variations in the E(1)–E(1a) distances among the noncentered $Ni_{10}P_2$ (3.17 Å), $Ni_{10}As_2$ (3.69 Å), and $Ni_{10}Sb_2$ (3.90 Å) cores are considerably greater than the variations in mean Ni–Ni distances of 4.90, 5.01, and 5.15 Å, respectively, among the five centrosymmetrically related pairs of Ni atoms. (3) The five independent intrapentagonal Ni–Ni distances within the E-capped nickel pentagons also increase uniformly as E increases in size, viz., from 2.61 Å (av) for E = P, to 2.69 Å (av) for E = As, to 2.78 Å (av) for E = Sb. (4) The five independent interpentagonal Ni–Ni distances between the E-capped pentagons of 2.50 Å (av) for E = P, 2.49 Å (av) for E = As, and 2.50 Å for E = Sb are invariant to the increased size of E.

These trends provide a logical explanation for our failure to isolate the homologous $[Ni_{10}(ER)_2(CO)_{18}]^{2-}$ dianions for E = Bi, as the intrapentagonal Ni–Ni distances would then be too long to support reasonable Ni–Ni bonding interactions.

According to Benfield and Johnson [34], the structures of many transition metal carbonyl clusters are merely the result of the insertion of a metal polyhedron within a regular or semi-regular polyhedron of carbonyl ligands. In **2** as well as in the analogous $[Ni_{10}(ER)_2(CO)_{18}]^{2-}$ dianions (E = P, As), each of the icosahedral $Ni_{10}E_2$ cores is similarly encompassed by a semi-regular 20-vertex polyhedron composed of 18 carbonyl oxygen atoms and two E-attached carbon atoms. This polyhedral ligand arrangement, presented in detail elsewhere [5], consists primarily of triangular and rectangular faces. Of particular interest is that the resulting analogous array of 10 terminal, four doubly, and four triply bridging carbonyl groups has a marked influence on the geometry of the $Ni_{10}E_2$ core, as shown in Table 9 by large variations of certain Ni–Ni bonds from mean distances under assumed D_{5d}-$\overline{1}0$ 2 *m* symmetry. These particular distortions in the geometry of a $Ni_{10}E_2$ core reduce its pseudo symmetry to C_{2h}-2/*m* which expectedly is the same pseudo symmetry exhibited by the 20-vertex ligand polyhedron.

Isolation and characterization of $Ni(CO)_3(SbClPh_2)$ and $Ni_2(CO)_4(Ph_2SbOSbPh_2)_2$ (3). Although a large number of monosubstituted, disubstituted, and trisubstituted tertiary phosphine derivatives of $Ni(CO)_4$ are known [35*–38], only a few monosubstituted $Ni(CO)_3L$ and disubstituted $Ni(CO)_2L_2$ stibine complexes (L = $SbPh_3$, $SbEt_3$, $SbClEt_2$) have been isolated and characterized by infrared spectral measurements [26]. These two types of $Ni(CO)_3L$ and $Ni(CO)_2L_2$ complexes (for a given L ligand) may be readily distinguished from each other by their infrared active vibrational carbonyl frequencies [26,36]. For example, an infrared spectrum for each of the above three nickel tricarbonyl stibine molecules displays a characteristic two-band carbonyl pattern with one frequency of range 2067–2082 cm^{-1} (A_1 mode)

and the other of range 1996–2020 cm^{-1} (E mode), whereas an infrared spectrum for each of the above three nickel dicarbonyl-bis(stibine) molecules exhibits a characteristic two-band carbonyl pattern with one frequency of range 2004–2034 cm^{-1} (A_1 mode) and the other of range 1948–1984 cm^{-1} (B_1 mode) [26].

Both $Ni(CO)_3(SbClPh_2)$ and **3** were obtained from the hexane-extracted mixture of products resulting from the reaction of $[Ni_6(CO)_{12}]^{2-}$ (**1**) with chlorodiphenylstibine. Although not isolated from solution, the existence of $Ni(CO)_3(SbClPh_2)$ in hexane solution is predicated upon its infrared spectrum (Fig. 2) with carbonyl bands at 2075(m) and 2005(s) cm^{-1} being similar to that given above [26] for the analogous $Ni(CO)_3(SbClEt_2)$ and $Ni(CO)_3(SbPh_3)$.

Yellow crystals of **3** isolated from a concentrated solution of the hexane extract were crystallographically and spectroscopically characterized. The structural determination of **3** represents the first X-ray study of a nickel-antimony carbonyl complex. The formation of the $Ph_2SbOSbPh_2$ ligand, whose stoichiometry was conclusively established by combined X-ray diffraction and mass spectral analyses, is a consequence of the partial hydrolysis of the chlorodiphenylstibine reagent. An infrared spectrum (Fig. 3) of **3** dissolved in THF gave two strong carbonyl bands at 2015 and 1960 cm^{-1}; these frequencies are virtually identical with those of 2016 and 1963 cm^{-1} reported [26] for $Ni(CO)_2(SbPh_3)_2$. It is noteworthy that yellow crystals were also isolated from the THF extract and tentatively identified as **3** from an infrared spectrum. Cyclic voltammetric measurements in THF solution showed that **3** undergoes only irreversible oxidation.

It is not surprising that no stibinido-bridged analogue of the known 34-electron $Ni_2(CO)_4(\mu_2\text{-}PR_2)_2$-type dimer (with two tetrahedral Ni^I linked by a Ni–Ni bond; R = Ph [39], Cy [40], t-Bu [41,42], the known 32-electron $Ni_2(CO)_3(\mu_2\text{-}PR_2)_2$-type dimer (with one trigonal-planar Ni^I and one tetrahedral Ni^I linked by a Ni–Ni bond; R = t-Bu [43]), or the known 36 electron $(OC)_3NiMe_2P\text{–}PMe_2Ni(CO)_3$-type dimer [44] was isolated. Any such nickel-stibine species would be much more unstable on the basis of both electronic and steric effects. In addition to the considerably weaker coordinating ability of the less basic Sb^{III} donor atoms relative to P^{III} donor atoms [37,45], intramolecular steric pressures would presumably preclude the existence of any hypothetical cyclo-Ni_2Sb_2 dimer due to the considerably larger Sb atoms imposing a much greater angular strain upon the four-membered Ni_2Sb_2 ring containing an electron-pair Ni–Ni bonding interaction.

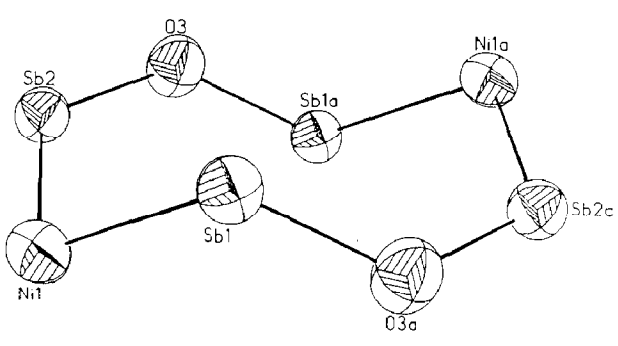

Fig. 6. The eight-membered $[NiSbOSb]_2$ ring in $Ni_2(CO)_4(\mu_2\text{-}Ph_2SbOSbPh_2)_2$ (**3**). Its centrosymmetric chair-like conformation is attributed to steric effects arising from the bulky Sb-attached phenyl rings.

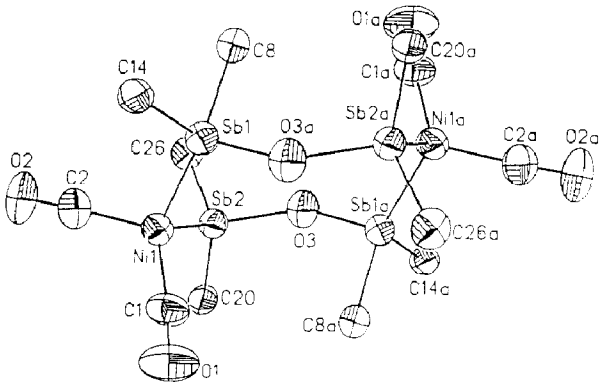

Fig. 7. Configuration of the $Ni_2(CO)_4(\mu_2\text{-}Ph_2SbOSbPh_2)_2$ molecule (**3**) possesses crystallographic C_i-$\bar{1}$ site symmetry. Only the Sb-attached carbon atom for each of the eight phenyl substituents is shown (for clarity).

Structural features of $Ni_2(CO)_4(\mu_2\text{-}Ph_2SbOSbPh_2)_2$ (3). This molecular compound (Fig. 6 and 7) can be envisioned as a metal dimer in which two $Ni(CO)_2$ fragments are connected by Ni–Sb bonds with two bridging $Ph_2SbOSbPh_2$ ligands. The resulting eight-membered cyclo-$(NiSbOSb)_2$ system of crystallographic C_i-$\bar{1}$ site symmetry possesses a chair-like conformation which is readily attributed to the bulky phenyl rings attached to the four antimony ring atoms. This complex is best viewed as a disubstituted $Ni(CO)_2L_2$ derivative of nickel tetracarbonyl in which two electron-donating Sb^{III} atoms have replaced two carbonyl groups around each zerovalent nickel atom. Its stability is presumably enhanced, relative to that of the known monomeric $Ni(CO)_2(SbPh_3)_2$, by the chelation effect in that both Sb^{III} donor atoms in each of the two bifunctional $Ph_2SbOSbPh_2$ ligands are coordinated to two different $Ni(CO)_2$ moieties.

The two independent Ni–Sb(1) and Ni–Sb(2) ring distances of 2.447(1) and 2.450(1) Å, respectively, are equal within experimental error, as are also the two independent Sb(1)–O(3a) and Sb(2)–O(3) ring distances of 1.941(7) and 1.944(7) Å, respectively.The two independent Ni–CO and C–O bond lengths of 1.768 (av) and 1.135 Å (av), respectively, are normal for a tetrahedral-like $Ni(CO)_2L_2$ complex.

A close examination of the four independent ring bond angles as well as the other 15 independent tetrahedral-like bond angles (Table 8) about the Ni(1), Ni(2), Sb(1), and Sb(2) atoms expectedly shows that the observed geometrical deformation of the $(NiSbOSb)_2$ ring from equivalent bond angles as well as the particular axial-equatorial orientations of the nickel-attached carbonyl and antimony-attached phenyl ligands (Figs. 5 and 6) are dictated by steric effects.

Comparative geometrical analysis of $Ni_2(CO)_4(\mu_2\text{-}Ph_2SbOSbPh_2)_2$ (3) with the "free" oxobis(diphenylstibine) ligand, $Ph_2SbOSbPh_2$ (4), and resulting implications. This nickel carbonyl dimer (**3**) is the first known "adduct" complex of the $Ph_2SbOSbPh_2$ molecule (**4**). An X-ray crystallographic analysis of oxobis(diphenylstibine) (**4**) reported by Bordner et al. [20] in 1974 revealed a crystallographically independent, discrete molecule with the two nonidentical but similar four-coordinate Sb atoms possessing experimentally equivalent Sb–O and Sb–C bond lengths of 1.970 (av) and 2.156 Å (av), respectively [46*,47]. Since the C–Sb–C and C–Sb–O bond angles are only slightly larger than 90°, it was concluded [20] that

the antimony lone-pair electrons are essentially *s* in character. The fact that a ^{121}Sb Mossbauer spectrum of **4** displayed two distinct absorption peaks was attributed to an extremely large asymmetric parameter (i.e., $\eta = 0.90$) in the electric field gradient at the ^{121}Sb nucleus [21].

A comparison of the molecular structures of **3** and "free" **4** is highly informative. A most striking feature is the significant increase in the two independent C–Sb–C bond angles from 94.6° (av) (range, 94.4(2)–94.9(3)°) in the "free" **4** [20] to 100.1° (av) (range, 97.7(3)–102.5(3)°) in **3**. Under the assumption that the C–Sb–C bond angles reflect only orbital contributions, it follows that the Sb–C bonds in **3** have greater valence 5*s* Sb orbital character than those in **4**. Further compelling evidence for greater 5*s* Sb orbital character in the four Sb–C bonds in **3** compared to that in **4** is given by the Sb–C distances of 2.120 Å (av) (range, 2.114(7)–2.126(6) Å) in **3** being markedly smaller than those of 2.156 Å (av) (range, 2.150(7)–2.166(7) Å) in **4**. In turn, these arguments reflect the notion that the hybridized lone-pair Sb orbital used in forming each Sb–Ni bond has less 5*s* (and more 5*p*) character than that of the lone-pair orbital of each Sb atom in "free" **4**.

Geometrical comparisons of $Cr(CO)_5(SbPh_3)$ [48] with the closely related "free" Sb(*p*-tolyl)$_3$ [49] and of bis(pentacarbonylchromium)-tetraphenyldistibine [50], $(OC)_5CrPh_2Sb–SbPh_2Cr(CO)_5$, with "free" tetraphenyldistibine [51], Sb_2Ph_4, show analogous bond-angle, bond-length trends [52*,53*] consistent with the above-stated bonding interpretation. Similar bonding arguments were used by Carty, Lappert, and co-workers [48] in analyzing the structural changes within the crystallographically isomorphous $Cr(CO)_5(EPh_3)$ series (E = P [54], As [48], Sb [48], Bi [48]).

The smaller symmetrical Sb–O bond lengths of 1.942 Å (av) in **3** compared to those of 1.970 Å (av) in "free" **4** may be correlated with the larger Sb–O–Sb bridge angle of 130.7(3)° in **3** compared to that of 122.1(3)° in "free" **4**. A similar trend between the Sb–O(bridge) distance and Sb–O–Sb bridge angle was observed for several oxybis(stibine) complexes containing trigonal-bipyramidally or octahedrally coordinated Sb^V atoms linked by a bridging oxygen atom [55,56].

Acknowledgments

This research was made possible by a grant from the National Science Foundation. We are particularly grateful to the Analytical Division, Nicolet Instruments Corporation (Madison, WI 53711-0370) for the use of the FTMS-2000 spectrometer. One author (A.B.) wishes to acknowledge the Icelandic Science Foundation, the University of Iceland Research Fund, and the Fulbright Foundation for travel funds. Another author (J. A. G.) wishes to acknowledge the Chemistry Department (UW-Madison) for an Alfred L. Wilds Undergraduate Scholarship in Chemistry during 1987–88. We also are most grateful to Dr. Bruce R. Adams (UW-Madison) for his assistance in carrying out the NMR measurements and to Dr. Kenneth J. Haller (presently at Oneida Research Services, Inc., Whitesboro, New York 13492) for helpful crystallographic advice. We are pleased to acknowledge the NSF Instruments Program which provided funds to the Chemistry Department (UW-Madison) for the purchase of the Bruker AM-360 and AM-500 NMR spectrometers.

References

1 J.C. Calabrese, L.F. Dahl, A. Cavalieri, P. Chini, P. Longoni, and S. Martinengo, J. Am. Chem. Soc., 96 (1974) 2616; (b) G. Longoni, P. Chini, and A. Cavalieri, Inorg. Chem., 15 (1976) 3025.

2 L.D. Lower and L.F. Dahl, J. Am. Chem. Soc., 98 (1976) 5046.

3 R.A. Montag, Ph.D. Thesis, University of Wisconsin-Madison, 1982; (b) R.A. Montag and L.F. Dahl, manuscript in preparation.

4 D.F. Rieck, R.A. Montag, T.S. McKechnie, and L.F. Dahl, J. Am. Chem. Soc., 108 (1986) 1330.

5 D.F. Rieck, A.D. Rae, and L.F. Dahl, Abstr. Papers, 190th Nat. meeting Am. Chem. Soc. Chicago, IL, September 1985; American Chemical Society: Washington, D.C., 1985; INOR 157; (b) D.F. Reick, Ph.D. Thesis, University of Wisconsin-Madison, 1986; (c) D.F. Rieck, A.D. Rae, J.A. Gavney, Jr. and L.F. Dahl, submitted for publication.

6 J.A. Gavney, Jr., R.E. DesEnfants, II, and L.F. Dahl, manuscript in preparation.

7 A.F. Wells, Structural Inorganic Chemistry, 5th edit., Oxford University Press, London, 1984, p. 69–71; (b) K.C.C. Kharas and L.F. Dahl, Ligand-Stabilized Metal Clusters: Structure, Bonding, Fluxionality, and the Metallic State, I. Prigogine, S.A. Rice (Eds.), Adv. Chem. Phys., John Wiley & Sons, New York, Vol. 70 (Part II), 1988, p. 1–43.

8 (a) M. Elian, M.M.L. Chen, D.M.P. Mingos, and R. Hoffmann, Inorg. Chem., 15 (1976) 1148; (b) R. Hoffmann, Science (Washington, D.C.), 211 (1981) 995; (c) R. Hoffmann, Angew. Chem., Int. Ed. Engl., 21 (1982) 711; (d) F.G.A. Stone, ibid., 23 (1984) 89; (e) T.A. Albright, Tetrahedron, 38 (1982) 1339.

9 An intriguing nickel carbonyl diphosphene cluster, $Ni_5(CO)_6[(Me_3Si)_2HCP{=}PCH(SiMe_3)_2]_2Cl$, was reported by Olmsted and Power [10] from the reaction of the sodium salt of the $[Ni_6(CO)_{12}]^{2-}$ dianion (**1**) with $P[CH(SiMe_3)_2]Cl_2$ in ether at room temperature. The tremendous steric influence of the R substituent of the main-group ER ligand on the main product generated is strikingly illustrated here in that the above dichlorophosphine reagent is related to $PhPCl_2$, which upon reaction with **1** produced $Ni_8(CO)_8(\mu_4\text{-}PPh)_6$ with a hexa-PhP-capping cubane Ni_8 core [2], by the formal substitution of the phenyl substituent with a much bulkier $CH(SiMe_3)_2$ one.

10 M.M. Olmsted and P.P. Power, J. Am. Chem. Soc., 106 (1984) 1495.

11 From a systematic stereochemical examination of the known $(OC)_9Co_3E(L)_n$ clusters, (E = hetero element) containing tetrahedral Co_3E cores, Schmid [12] pointed out that the size of E has a limiting effect on the existence of such clusters (i.e., no such species have so far been prepared in which the covalent radius of the E atom exceeds 1.3 Å). Schmid [12] further observed that hetero E atoms bearing several L ligands favor carbonyl bridges between cobalt atoms, whereas those bearing only one L ligand or none permit terminal bonding of all the carbonyl groups.

12 G. Schmid, Angew. Chem. Int. Ed. Engl., 17 (1978) 392.

13 Mingos [14] utilized an extension of the cone-angle concept, developed by Tolman [15] to evaluate steric effects of phosphorus ligands in organometallic complexes and homogeneous catalysts, to assess in a semiquantitative fashion the relative importance of steric effects in a variety of metal carbonyl and metal cyclopentadienyl clusters.

14 D.M.P. Mingos, Inorg. Chem., 21 (1982) 465.

15 C.A. Tolman, Chem. Rev., 77 (1977) 313.

16 G.O. Doak and L.D. Freeman, Compounds of Arsenic, Antimony, and Bismuth, Wiley-Interscience, 1970, p. 389–401, and ref. therein.

17 N.N. Greenwood and A. Earnshaw, Chemistry of the Elements, Pergamon Press, New York, N.Y., 1984, p. 695.

18 H. Schmidt, Liebigs. Ann. Chem., 421 (1920) 174.

19 (a) H.H. Jaffe and G.O. Doak, J. Am. Chem. Soc., 71 (1949) 602; (b) 72 (1950) 3027.

20 J. Bordner, B.C. Andrews, and G.G. Long, Cryst. Struct. Comm., 3 (1974) 53.

21 (a) L.H. Bowen, G.G. Long, J.G. Stevens, N.C. Campbell, and T.B. Brill, Inorg. Chem., 13 (1974) 1787; (b) S.W. Hedges and L.H. Bowen, J. Chem. Phys., 67 (1977) 4706.

22 M. Wieber, D. Wirth, and I. Fetzer, Z. Anorg. Allg. Chem., 505 (1983) 134.

23 (a) A. Michaelis and A. Marquardt, Liebigs Ann. Chem., 251 (1889) 323; (b)F. Challenger and C.F. Allpress, J. Chem. Soc., 119 (1921) 913, and ref. therein; (c) H. Gilman and H.L. Yablunsky, J. Am. Chem. Soc., 63 (1941) 207.

24 (a) G.O. Doak and L.D. Freeman, Compounds of Arsenic, Antimony, and Bismuth, Wiley-Interscience, New York, 1970, p. 419–423, and ref. therein; (b) p. 437–439, and ref. therein.

25 (a) G. Bouquet, A. Loutellier, and M. Bigorgne, J. Mol. Struct., 1 (1968) 211; (b) M. Bigorgne, Bull. Soc. Chim. Fr., (1960) 1986.
26 D. Benlian and M. Bigorgne, Bull. Soc. Chim. Fr., (1963) 1583.
27 (a) Empirical corrections based on ψ-scan measurements at different azimuthal angles were calculated with the XEMP program (SHELXTL). (b) Empirical absorption corrections [28] were computed from the ΔF values by use of an option in the least-squares program RAELS [29]. These corrections, based upon an empirical spherical harmonic model, are similar to those used by Hope [27c]. (c) Empirical absorption corrections were obtained via the Hope–Moezzi ABSORPTION program (sent to L.F. Dahl from H. Hope, Feb. 1984) which utilizes an empirical absorption tensor from an expression relating $|F_0|$ and $|F_c|$.
28 A.D. Rae, The Refinability of Absorption Corrections, presented at the Ann. Meeting Am. Cryst. Assoc., McMaster University, Hamilton, Ontario, Canada, June 22–27, 1986; Abstr. PA14.
29 A.D. Rae, RAELS-A Comprehensive Least-Squares Program, University of New South Wales, Kensington, 1976; Adapted for a Harris/7 computer by A.D. Rae, University of Wisconsin, Madison, 1983.
30 International Tables for X-Ray Crystallography, Vol. IV, Kynoch Press, Birmingham, England, 1974, p. 149; p. 155–157.
31 (a) P. Main, L. Lessinger, M.M. Woolfson, G. Germain, and J.-P. Declerq, MULTAN-78; (b) G. Germain, P. Main, M.M. Woolfson, Acta. Crystallorg., A, 27 (1971) 368.
32 A.D. Rae, Acta Crystallorg., A, 31 (1975) 570.
33 G. Sheldrick, RANT. This random-angle and tangent program is included in the SHELXTL, 1984, program package.
34 (a) R.E. Benfield and B.F.G. Johnson, J. Chem. Soc., Dalton Trans., (1980) 1743; (b) B.F.G. Johnson and R.E. Benfield, in G. Geoffroy (Ed.), Topics in Inorganic and Organometallic Stereochemistry, John Wiley & Sons, New York, Vol. 12, 1981, p. 253–335.
35 From a comprehensive study involving a semiquantitative estimation of the extent of substitution of the carbonyl ligands in $Ni(CO)_4$ by 14 different tertiary phosphine L ligands, Tolman [36] provided convincing evidence that the stabilities of the resulting $Ni(CO)_3L$, $Ni(CO)_2L_2$, or $Ni(CO)L_3$ complexes are determined in most cases by the sizes of the L ligands rather than by electronic effects. Tolman [36] concluded "that double bonding between nickel and phosphorus, if it does occur in these complexes, is much less important in determining the relative stability of the complexes than the dominant steric effects."
36 C.A. Tolman, J. Am. Chem. Soc., 92 (1970) 2956.
37 G. Booth, Adv. Inorg. Chem. Radiochem., 6 (1964) 1.
38 J.C. Cloyd, Jr. and C.A. McAuliffe, in C.A. McAuliffe (Ed.), Transition Metal Complexes of Phosphorus, Arsenic, and Antimony Ligands, John Wiley and Sons, New York, 1973, p. 245–246, and ref. therein.
39 (a) J.A.J. Jarvis, R.H.B. Mais, P.G. Owston, and D.T. Thompson, J. Chem. Soc. A, (1970) 1867; (b) R.G. Hayter, Inorg. Chem., 3 (1964) 711.
40 C.F. Noble, G. Vasapollo, P. Giannoccaro, and A. Sacco, Inorg. Chim. Acta, 48 (1981) 261.
41 A.M. Arif, R.A. Jones, and S.T. Schwab, J. Coord. Chem., 16 (1987) 51.
42 R.E. DesEnfants, II, and L.F. Dahl, unpublished results.
43 R.A. Jones, A.L. Stuart, J.L. Atwood, and W.E. Hunter, Organometallics, 2 (1983) 874.
44 R.H.B. Mais, P.G. Owston, D.T. Thompson, and A.M. Wood, J. Chem. Soc. A, (1967) 1744.
45 G.O. Doak and L.D. Freeman, Compounds of Arsenic, Antimony, and Bismuth, Wiley-Interscience, New York, 1970, p. 1–16, and ref. therein.
46 The solid-state structure of "free" $Ph_2SbOSbPh_2$ (**4**) is crystallographically isomorphous with that of $Ph_2AsOAsPh_2$ whose geometry was determined by Cullen and Trotter [47] in 1963. Although their results are based on only two-dimensional X-ray film data and hence are relatively imprecise, it is noteworthy that the six determined C–As–C and O–As–C bond angles of 98–106° range are significantly larger than those found [20] in "free" $Ph_2SbOSbPh_2$ (**4**). This variation expectedly correlates with the E–C and E–O electron-pair bonds having greater valence *s* E orbital character and conversely, the lone-pair hybrid orbital of E having less *s* AO (and more *p* AO) character for E = As than for E = Sb.
47 W.R. Cullen and J. Trotter, Can. J. Chem., 41 (1963) 2983.
48 A.J. Carty, N.J. Taylor, A.W. Coleman, and M.F. Lappert, J. Chem. Soc. Chem. Comm., (1979) 639.
49 A.N. Sobolev, I.P. Romm, V.K. Belsky, and E.N. Guryanova, J. Organomet. Chem., 179 (1979) 153.

50 J. v. Seyerl and G. Huttner, Cryst. Struct. Comm., 9 (1980) 1099.
51 K. von Deuten und D. Rehder, Cryst. Struct. Comm., 9 (1980) 167.
52 The C–Sb–C bond angle of 97.3(1)° in Sb(*p*-tolyl)$_3$ [49] is smaller than those (99.2° (av); range 98.4(0)–101.8(0)°) in $Cr(CO)_5(SbPh_3)$ [48], whereas the Sb–C bond length of 2.141(3) Å in the "free" tri-*p*-tolylantimony molecule [49] is larger than those (2.133 Å (av); range 2.130(3)–2.136(2) Å) in $Cr(CO)_5(SbPh_3)$ [48].
53 The C–Sb–C bond angle of 94.4(2)° in Sb_2Ph_4 [51] of crystallographic C_i-$\bar{1}$ site symmetry is smaller than that of 101.0(3)° in $(OC)_5CrPh_2Sb–SbPh_2Cr(CO)_5$ [50] of crystallographic C_i-$\bar{1}$ site symmetry, whereas the two independent Sb–C bond lengths (2.156 Å (av); range 2.146(4)–2.167(4) Å) in "free" Sb_2Ph_4 [51] are larger than those (2.139 Å (av); range 2.133(7)–2.145(7) Å) in $(OC)_5CrPh_2Sb–SbPh_2Cr(CO)_5$ [50]. The Sb–Sb single-bond distance of 2.837(1) Å in Sb_2Ph_4 increases to 2.866(1) Å upon formation of $(OC)_5CrPh_2Sb–SbPh_2Cr(CO)_5$. The independent Sb–Cr bond length of 2.626(1) Å in this bis(pentacarbonylchromium)tetraphenyldistibine adduct is virtually identical to that of 2.6170(3) Å in $Cr(CO)_5(SbPh_3)$ [48].
54 (a) H.J. Plastas, J.M. Stewart, and S.O. Grim, J. Am. Chem. Soc., 91 (1969) 4326; (b) H.J. Plastas, J.M. Stewart, and S.O. Grim, Inorg. Chem., 12 (1973) 265.
55 I.E. Pokrovskaya, V.A. Dodonov, Z.A. Starikova, E.N. Kanunnikova, T.M. Shchegoleva, and G.P. Lebedeva, J. General Chem., USSR, 51 (1981) 1056, and ref. therein.
56 F. Ebina, A. Ouchi, Y. Yoshino, S. Sato, and Y. Saito, Acta Crystallogr., B, 34 (1978) 2134, and ref. therein.